J|A|C|S
ARTICLES
Published on Web 02/07/2006

Adding a New Dimension to the Investigation of Platinum-Mediated Arene C−H Activation Reactions Using 2D NMR Exchange Spectroscopy. Dynamics of Pt(II) Phenyl/Benzene Site Exchange

Bror Johan Wik, Martin Lersch, Alexander Krivokapic, and Mats Tilset*

Contribution from the Department of Chemistry, University of Oslo, P.O. Box 1033 Blindern, N-0315 Oslo, Norway

Received October 7, 2005; E-mail: mats.tilset@kjemi.uio.no

Abstract: Protonation of (N−N)$PtPh_2$ (**1**; N−N = diimine ArN=CMe−CMe=NAr with Ar = 2,6-$Me_2C_6H_3$ (**a**), 2,4,6-$Me_3C_6H_2$ (**b**), 4-Br-2,6-$Me_2C_6H_2$ (**c**), 3,5-$Me_2C_6H_3$ (**d**), and 4-$CF_3C_6H_4$ (**e**)) in the presence of MeCN at ambient temperature generates (N−N)Pt(Ph)$(NCMe)^+$ (**2**). At −78 °C, protonation of **1a** yielded (N−N)$PtPh_2$(H)$(NCMe)^+$ (**3a**), which produced benzene and **2a** at ca. −40 °C. Protonation of **1a**−**e** in CD_2Cl_2/Et_2O-d_{10} furnished (N−N)Pt$(C_6H_5)(\eta^2-C_6H_6)^+$ (**4a**−**e**). The π-benzene complexes **4a**−**c**, sterically protected at Pt, eliminate benzene at ca. 0 °C. The sterically less protected **4d**−**e** lose benzene already at −30 °C. SST and 2D EXSY NMR demonstrate that phenyl and π-benzene ligand protons undergo exchange with concomitant symmetrization of the diimine ligand, most likely via oxidative insertion of Pt into a C−H bond of coordinated benzene. The kinetics of the exchange processes for **4a**−**c** were probed by quantitative EXSY spectroscopy, resulting in $\Delta H^{\ddagger}$ of 70−72 kJ mol^{-1} and $\Delta S^{\ddagger}$ of 37−48 J K^{-1} mol^{-1}. A large, strongly temperature-dependent H/D kinetic isotope effect (9.7 at −34 °C; 6.9 at −19 °C) was measured for the dynamic behavior of **4a** versus **4a**-d_{10}, consistent with the proposed π-benzene C−H bond cleavage. The fact that the π-benzene complex **4a** is thermally more robust in the absence of MeCN than is the Pt(IV) hydridodiphenyl complex **3a** in the presence of MeCN agrees with the notion that arene elimination from Pt(IV) hydridoaryl complexes occurs via Pt(II) π-arene intermediates that eliminate the hydrocarbon associatively, in this case, promoted by MeCN. Compounds **1a**, **1b**, **1d**, **2a**, and **2b** have been crystallographically characterized.

Introduction

Efficient, selective, and direct functionalization of hydrocarbons by homogeneous transition-metal catalysts under mild conditions remains a most difficult challenge.[1−3] In addition to their potentially enormous economic consequences, new processes may also give rise to cleaner and more efficient alternatives to existing technology.[1−3] Extensive research efforts have targeted the hydrocarbon C−H bond activation and functionalization, as evidenced by numerous recent reviews.[4−10] Garnett and Hodges[11,12] demonstrated that aqueous Pt(II) salts were capable of activating aromatic C−H bonds, and the Shilov group[7,13,14] established shortly thereafter that aliphatic C−H bonds can also be activated by aqueous Pt(II) salts. The mechanisms of C−H activation at Pt have been vigorously investigated for the Shilov system and for organometallic model systems using a plethora of experimental and calculational methods, and these efforts have been extensively reviewed.[4,5,8]

Despite the fact that arene C−H bonds are considerably stronger than alkane C−H bonds, oxidative addition of arene C−H bonds is thermodynamically favored relative to alkene C−H bonds because of the formation of a strong metal−aryl bond.[15,16] There is substantial evidence that oxidative addition of arenes at an unsaturated metal center usually, although not without exceptions,[17,18] proceeds via η^2-(C,C) precomplexation of the arene,[8,19−27] probably followed by an arene "slip" to an

(1) Labinger, J. A. *J. Mol. Catal. A* **2004**, *220*, 27−35.
(2) Labinger, J. A.; Bercaw, J. E. *Nature* **2002**, *417*, 507−514.
(3) Periana, R. A.; Bhalla, G.; Tenn, W. J. I.; Young, K. J. H.; Liu, X. Y.; Mironov, O.; Jones, C.; Ziatdinov, V. R. *J. Mol. Catal. A* **2004**, *220*, 7−25.
(4) Lersch, M.; Tilset, M. *Chem. Rev.* **2005**, *105*, 2471−2526.
(5) Fekl, U.; Goldberg, K. I. *Adv. Inorg. Chem.* **2003**, *54*, 259−320.
(6) Arndtsen, B. A.; Bergman, R. G.; Mobley, T. A.; Peterson, T. H. *Acc. Chem. Res.* **1995**, *28*, 154−162.
(7) Shilov, A. E.; Shul'pin, G. B. *Chem. Rev.* **1997**, *97*, 2879−2932.
(8) Stahl, S. S.; Labinger, J. A.; Bercaw, J. E. *Angew. Chem., Int. Ed.* **1998**, *37*, 2181−2192.
(9) Crabtree, R. H. *J. Chem. Soc., Dalton Trans.* **2001**, 2437−2450.
(10) Crabtree, R. H. *J. Organomet. Chem.* **2004**, *689*, 4083−4091.
(11) Garnett, J. L.; Hodges, R. J. *J. Am. Chem. Soc.* **1967**, *89*, 4546−4547.
(12) Hodges, R. J.; Garnett, J. L. *J. Phys. Chem.* **1968**, *72*, 1673−1682.
(13) Gol'dshleger, N. F.; Tyabin, M. B.; Shilov, A. E.; Shteinman, A. A. *Zh. Fiz. Khim.* **1969**, *43*, 2174−2175.
(14) Shilov, A. E. *Activation and catalytic reactions of saturated hydrocarbons in the presence of metal complexes*; Kluwer Academic: Dordrecht, The Netherlands, 2000.
(15) Halpern, J. *Inorg. Chim. Acta* **1985**, *100*, 41−48.
(16) Jones, W. D.; Feher, F. J. *J. Am. Chem. Soc.* **1984**, *106*, 1650−1663.
(17) Vigalok, A.; Uzan, O.; Shimon, L. J. W.; Ben-David, Y.; Martin, J. M. L.; Milstein, D. *J. Am. Chem. Soc.* **1998**, *120*, 12539−12544.
(18) Peterson, T. H.; Golden, J. T.; Bergman, R. G. *J. Am. Chem. Soc.* **2001**, *123*, 455−462.
(19) Chin, R. M.; Dong, L.; Duckett, S. B.; Jones, W. D. *Organometallics* **1992**, *11*, 871−876.
(20) Chin, R. M.; Dong, L.; Duckett, S. B.; Partridge, M. G.; Jones, W. D.; Perutz, R. N. *J. Am. Chem. Soc.* **1993**, *115*, 7685−7695.
(21) Cronin, L.; Higgitt, C. L.; Perutz, R. N. *Organometallics* **2000**, *19*, 672−683.

10.1021/ja056694z CCC: $33.50

Scheme 1

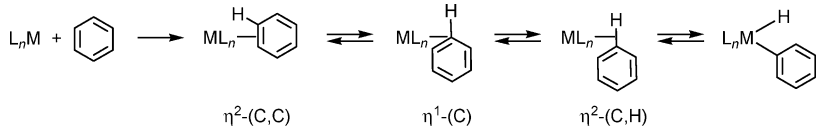

Scheme 2

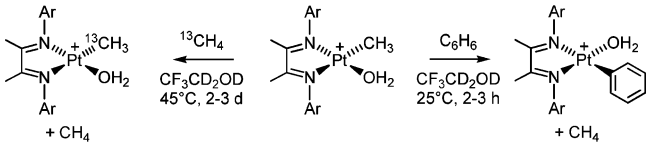

η^2-(C,H)[17,23,28] or even η^1-(C)[29] coordination mode from which the oxidative cleavage of the C−H bond occurs (Scheme 1). The fluxional behavior commonly depicted by η^2-arenes in combination with possibly rapid and reversible slippage and oxidative cleavage reactions constitutes an essential part of the dynamic processes that are the focus of this work.

We reported some time ago[30] that cationic Pt(II) diimine complexes, (N−N)Pt(Me)$(H_2O)^+$ (N−N = diimine ArN═CR−CR═NAr with R = H/Me; Ar = substituted aryl), are capable of activating aromatic, benzylic, and aliphatic C−H bonds according to Scheme 2. A series of contributions by us[28,31] and others[32−35] have addressed the mechanism of aromatic C−H activation at cationic Pt(II) diimine complexes and related Pt(II) species bearing bidentate ligands.[36−44] Mechanistic studies of benzene activation at (N−N)Pt species have been conducted in trifluoroethanol (TFE), a solvent which has been particularly useful because it is poorly coordinating, thus readily displaced by the hydrocarbon, and also does not degrade the reactive Pt complexes in undesired side reactions. The general mechanism for benzene activation that is depicted in Scheme 3 has emerged. Substitution of π-benzene for an aqua ligand occurs as a solvent-assisted process (a and b) for which there is evidence that both steps occur associatively.[33] The aqua and TFE complexes coexist in TFE solution. The π-benzene complex has not been directly observed under actual C−H activating conditions, as it is thermodynamically uphill relative to the solvento species, but has been independently generated and observed by NMR at low temperatures.[28] The Pt(II) center oxidatively inserts into a C−H bond of the π-benzene complex, presumably via (step c) an unobserved η^2-(C,H) benzene complex that proceeds with the oxidative cleavage (d). The resulting five-coordinate Pt(IV) species may be stabilized by coordinating a weakly bonded solvent molecule (e) or proceed by C−H reductive coupling (f) to yield the Pt(II) σ-methane complex, which finally furnishes the Pt(II) phenyl products by associative displacement of coordinated methane (g).

Zhong et al.[32] have conducted a thorough investigation of the ligand electronic and steric effects in benzene activation at a series of (N−N)Pt(Me)$(H_2O)^+$ complexes in TFE. Although the same rate law was obeyed in all cases, two distinctly different reactivity patterns were recognized when diimines of the type ArN═C(Me)-C(Me)═NAr were utilized. When the diimine N-aryl groups were sterically undemanding (bearing H atoms in the 2 and 6 positions), the kinetics exhibited a significant k_H/k_D isotope effect of ca. 2.0 in reactions of C_6H_6 versus C_6D_6. This was accompanied by only a small extent of H/D scrambling from C_6D_6 into the methane product or Pt−methyl group of unconsumed reactant. This is consistent with rate-limiting C−H oxidative cleavage (step d). On the other hand, when the N-aryl groups were 2,6-dimethyl-substituted, the k_H/k_D isotope effects were near unity, and significant scrambling of D from C_6D_6 occurred into the methane produced and the Pt−methyl group of unreacted Pt complex. This is consistent with rate-limiting benzene coordination (a, b) in the sterically demanding systems. The extensive isotopic scrambling can then be rationalized if steps c, d, and f (enclosed within the dotted frame in Scheme 3) are reversible and have lower activation barriers than the hydrocarbon-releasing steps, the associative substitutions g and b (the latter in reverse). Isotope exchange between Pt−Me and C_6D_6 has been observed in other C−H activating Pt systems as well.[45−47]

It has been established that isotope exchange occurs rapidly between Pt−CH_3 and Pt−D ligands in transient (N−N)Pt-$(CH_3)_2D^+$ species generated by treatment of (N−N)PtMe_2 precursors and DOTf at ambient temperature.[48] These isotope exchange processes, which signal repeated C−H reductive coupling/oxidative cleavage events without intervening hydrocarbon release from the metal, occur readily on experimental time scales of at most a few minutes in the NMR-tube experiments that are commonly preferred for these studies. Evidence for repeated C−H bond-forming and -breaking reactions between Pt hydrides and Pt aryl groups was also provided by the observation that protonolysis of (N−N)Pt-(*o*-tolyl)$_2$ in TFE produced mostly (N−N)Pt(*m*-tolyl)$(solv)^+$ and

(22) Iverson, C. N.; Lachicotte, R. J.; Mueller, C.; Jones, W. D. *Organometallics* **2002**, *21*, 5320−5333.
(23) Churchill, D. G.; Janak, K. E.; Wittenberg, J. S.; Parkin, G. *J. Am. Chem. Soc.* **2003**, *125*, 1403−1420.
(24) Jones, W. D.; Feher, F. J. *J. Am. Chem. Soc.* **1986**, *108*, 4814−4819.
(25) Jones, W. D.; Dong, L. *J. Am. Chem. Soc.* **1989**, *111*, 8722−8723.
(26) Cordone, R.; Taube, H. *J. Am. Chem. Soc.* **1987**, *109*, 8101−8102.
(27) Sweet, J. R.; Graham, W. A. G. *J. Am. Chem. Soc.* **1983**, *105*, 305−306.
(28) Johansson, L.; Tilset, M.; Labinger, J. A.; Bercaw, J. E. *J. Am. Chem. Soc.* **2000**, *122*, 10846−10855.
(29) Krumper, J. R.; Gerisch, M.; Magistrato, A.; Rothlisberger, U.; Bergman, R. G.; Tilley, T. D. *J. Am. Chem. Soc.* **2004**, *126*, 12492−12502.
(30) Johansson, L.; Ryan, O. B.; Tilset, M. *J. Am. Chem. Soc.* **1999**, *121*, 1974−1975.
(31) Johansson, L.; Ryan, O. B.; Rømming, C.; Tilset, M. *J. Am. Chem. Soc.* **2001**, *123*, 6579−6590.
(32) Zhong, H. A.; Labinger, J. A.; Bercaw, J. E. *J. Am. Chem. Soc.* **2002**, *124*, 1378−1399.
(33) Procelewska, J.; Zahl, A.; van Eldik, R.; Zhong, H. A.; Labinger, J. A.; Bercaw, J. E. *Inorg. Chem.* **2002**, *41*, 2808−2810.
(34) Gerdes, G.; Chen, P. *Organometallics* **2003**, *22*, 2217−2225.
(35) Heyduk, A. F.; Driver, T. G.; Labinger, J. A.; Bercaw, J. E. *J. Am. Chem. Soc.* **2004**, *126*, 15034−15035.
(36) Thomas, J. C.; Peters, J. C. *J. Am. Chem. Soc.* **2001**, *123*, 5100−5101.
(37) Harkins, S. B.; Peters, J. C. *Organometallics* **2002**, *21*, 1753−1755.
(38) Song, D.; Wang, S. *Organometallics* **2003**, *22*, 2187−2189.
(39) Thomas, J. C.; Peters, J. C. *J. Am. Chem. Soc.* **2003**, *125*, 8870−8888.
(40) Iverson, C. N.; Carter, C. A. G.; Baker, R. T.; Scollard, J. D.; Labinger, J. A.; Bercaw, J. E. *J. Am. Chem. Soc.* **2003**, *125*, 12674−12675.
(41) Song, D.; Jia, W. L.; Wang, S. *Organometallics* **2004**, *23*, 1194−1196.
(42) Vedernikov, A. N.; Pink, M.; Caulton, K. G. *Inorg. Chem.* **2004**, *43*, 3642−3646.
(43) Liang, L.-C.; Lin, J.-M.; Lee, W.-Y. *Chem. Commun.* **2005**, 2462−2464.
(44) Driver, T. G.; Day, M. W.; Labinger, J. A.; Bercaw, J. E. *Organometallics* **2005**, *24*, 3644−3654.
(45) Stahl, S. S.; Labinger, J. A.; Bercaw, J. E. *J. Am. Chem. Soc.* **1995**, *117*, 9371−9372.
(46) Holtkamp, M. W.; Labinger, J. A.; Bercaw, J. E. *J. Am. Chem. Soc.* **1997**, *119*, 848−849.
(47) Vedernikov, A. N.; Caulton, K. G. *Chem. Commun.* **2003**, 358−359.
(48) Johansson, L.; Tilset, M. *J. Am. Chem. Soc.* **2001**, *123*, 739−740.

Scheme 3

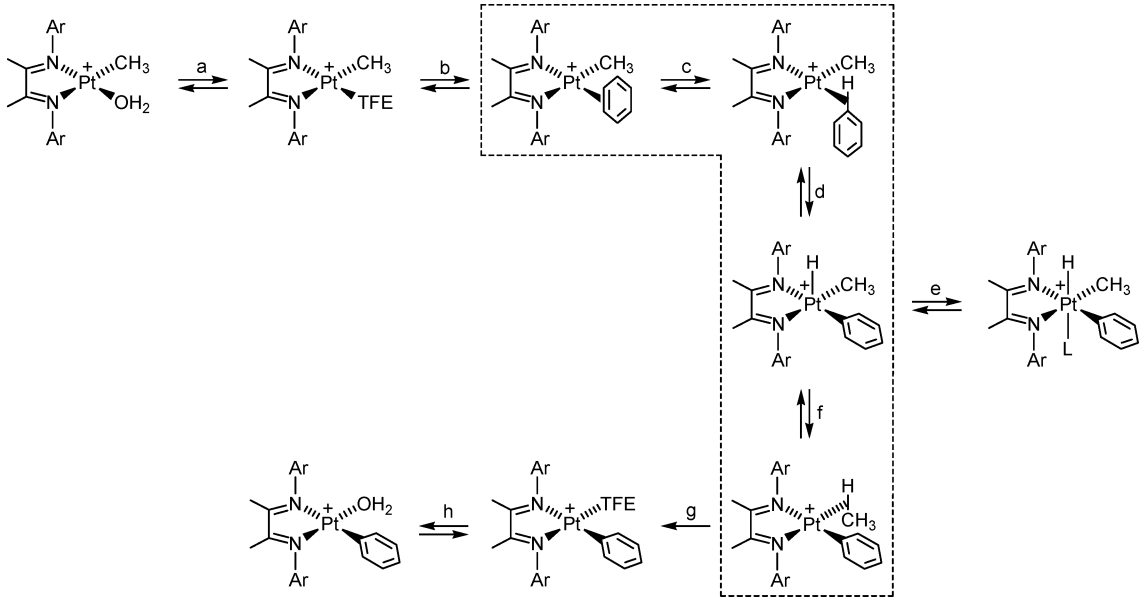

(N−N)Pt(*p*-tolyl)(solv)$^+$ products. Isomerization was seen also from the *m*-tolyl and *p*-tolyl analogues.[31] The extent of isomerization was inhibited by acetonitrile addition, which is evidence that toluene release from incipient (N−N)Pt(π-toluene)(tolyl)$^+$ species has to be associative. Finally, C_6H_5D as well as $C_6H_4D_2$ was produced by treatment of (tBu$_2$bpy)PtPh$_2$ with DBF_4 in CD_3OD.[49] Numerous other examples of H/D scrambling between hydride and methyl sites, the perhaps most tell-tale proof of involvement of σ-methane intermediates, have been reported for Pt(IV) hydridoalkyl complexes, as summarized in a recent review.[4]

The Jones and Perutz groups have thoroughly investigated the dynamic behavior of Cp(*)Rh(PMe$_3$)(η^2-arene) and Cp(*)-Rh(PMe$_3$)(H)(aryl) complexes (where Cp(*) = Cp or Cp*). SST (spin-saturation transfer) measurements were applied to probe the exchange of hydrogens between the ortho, meta, and para sites of CpRh(PMe$_3$)(H)(C_6H_5) and the interconversion between CpRh(PMe$_3$)(η^2-*p*-xylene) and CpRh(PMe$_3$)(H)(2,5-Me$_2$C$_6$H$_3$).[16] The interconversion of Cp*Rh(PMe$_3$)(η^2-naphthalene) to the corresponding aryl hydride was probed by SST.[20,21,50] In a recent contribution that is directly relevant to the Pt chemistry, Jones and co-workers have reported that the (^{t}Bu$_2$PCH$_2$P^{t}Bu$_2$)Pt fragment gives η^2-arene complexes with electron-deficient arenes. Some of these η^2-arene complexes undergo C−H oxidative cleavage, and there is evidence that some of these reactions are reversible at temperatures above ambient.[22]

Templeton and co-workers have described the rapid site exchange between hydride, phenyl, and π-benzene ligands bonded at the Tp′Pt moiety. Protonation of (κ^3-Tp′)PtH$_2$Ph occurs at a pyrazole-N atom of the Tp′ ligand to yield the Pt(II) benzene hydride complex (κ^2-HTp′)Pt(η^2-C_6H_6)H$^+$ (Scheme 4, left structure), crystallographically characterized as its BAr_f^- salt.[51] NMR line-broadening measurements demonstrated that H atom exchange occurs between the hydride and phenyl sites

Scheme 4

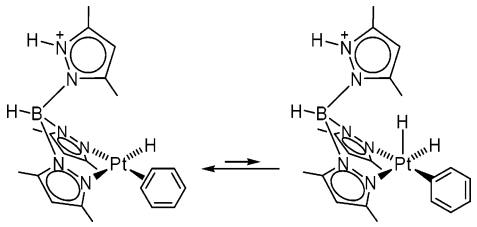

Scheme 5

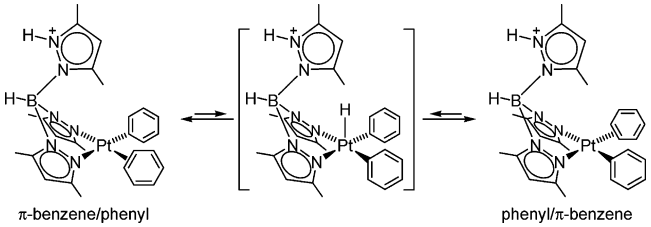

at a rate of 47 s^{-1} at −21 °C, presumably via the intermediacy of the Pt(IV) dihydridophenyl complex (right structure). Variable-temperature SST measurements[52] provided the kinetic parameters ($\Delta H^‡$ = 49(2) kJ mol^{-1}, $\Delta S^‡$ = −16(8) J K^{-1} mol^{-1}), and a kinetic isotope effect (k_H/k_D = 3.0) was determined at −14 °C by comparison with (κ^2-HTp′)Pt(η^2-C_6D_6)D$^+$. In a related system, protonation of (κ^3-Tp′)PtPh$_2$H furnished (κ^2-HTp′)Pt(C_6H_5)(η^2-C_6H_6)$^+$.[52] An SST investigation demonstrated H exchange between the phenyl and π-benzene sites in this Pt(II) complex ($\Delta G^‡$ = 54 kJ mol^{-1}), presumably via the Pt(IV) hydride (κ^2-HTp′)PtPh$_2$H$^+$ (Scheme 5). In this case, k_H/k_D = 4.7 at −32 °C by comparison with (κ^2-HTp′)Pt(C_6D_5)(η^2-C_6D_6)$^+$. Recently, reversible interconversion between the Pt(II) and Pt(IV) complexes (κ^2-HTp′)Pt(R)(η^2-C_6H_6)$^+$ (R = H, Ph) and (κ^2-HTp′)Pt(R)(C_6H_5)(H)(NCR′)$^+$ has been established. It was demonstrated that the preference for Pt(II) versus Pt(IV) can be tuned by the absence/presence of an extra coordinating ligand (in this case a nitrile) and by the identity of this ligand.[53]

(49) Ong, C. M.; Jennings, M. C.; Puddephatt, R. J. *Can. J. Chem.* **2003**, *81*, 1196−1205.
(50) Belt, S. T.; Dong, L.; Duckett, S. B.; Jones, W. D.; Partridge, M. G.; Perutz, R. N. *J. Chem. Soc., Chem. Commun.* **1991**, 266−269.
(51) Reinartz, S.; White, P. S.; Brookhart, M.; Templeton, J. L. *J. Am. Chem. Soc.* **2001**, *123*, 12724−12725.
(52) Norris, C. M.; Reinartz, S.; White, P. S.; Templeton, J. L. *Organometallics* **2002**, *21*, 5649−5656.
(53) Norris, C. M.; Templeton, J. L. *Organometallics* **2004**, *23*, 3101−3104.

Scheme 6

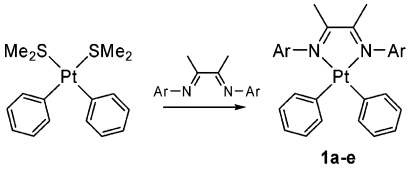

Compd	Ar
1a	2,6-$Me_2C_6H_3$
1b	2,4,6-$Me_3C_6H_2$
1c	4-Br-2,6-$Me_2C_6H_2$
1d	3,5-$Me_2C_6H_3$
1e	4-$CF_3C_6H_4$

Recently, quantitative 2D EXSY spectroscopy[54] has emerged to become a powerful tool for quantitative kinetics in dynamic systems. For example, 2D EXSY measurements have been applied to investigate various dynamic processes in Cp*Rh-(PMe_3)(η^2-naphthalene),[21] CpRe(CO)$_2$(η^2-1,4-$C_6H_4F_2$),[55] (PCy_3)$_2$-Pt(H)(SiR_3),[56] (κ^2-bis(imino)pyridine)PtMe_3X complexes,[57] Rh dihydrides,[58] and β-diketiminato alkyl scandium cations.[59] Neither of these apply to hydride/alkyl or hydride/aryl site exchange processes of relevance to C−H activation.

In this contribution, we describe the low-temperature protonation chemistry of (N−N)PtPh_2 complexes, where a choice between Pt(II) and Pt(IV) products is available depending on the reaction conditions. In the absence of strongly bonded ligands, Pt(II) phenyl/π-benzene complexes (N−N)Pt(C_6H_5)-(η^2-C_6H_6)$^+$ are formed. H atom exchange between the phenyl and π-benzene sites is demonstrated by SST and ^{1}H−^{1}H 2D EXSY spectroscopy. The kinetics of the exchange processes are established by quantitative 2D EXSY measurements. This appears to be the first time that this powerful method is applied to the study of C−H activation reactions within the coordination sphere of a metal.

Results

I. Synthesis and Characterization of Metal Complexes. The air- and moisture-stable diimine platinum diphenyl complexes **1a**−**e** (Scheme 6) were prepared in good yields by stirring a solution of (Me_2S)$_2$PtPh_2 and the diimine ligand (N−N) in toluene at ambient temperature according to previously published procedures.[28] The (N−N)PtPh_2 complexes were characterized by ^{1}H, ^{13}C, and ^{195}Pt NMR spectroscopy as well as elemental analysis. The structures of compounds **1a**, **1b**, and **1d** were confirmed by X-ray crystallography (vide infra). The C_{2v} symmetry of the molecules is evident from the spectroscopic data (see Experimental Section).

II. Protonation of (N−N)PtPh_2 Complexes. A. Protonation in the Presence of Acetonitrile at Ambient Temperature. Treatment of the (N−N)PtPh_2 complexes **1a**−**e** with triflic acid (HOTf) or HBF_4·Et_2O in acetonitrile at ambient temperature led to rapid conversion to the corresponding monophenyl solvento cations (N−N)Pt(Ph)(NCMe)$^+$ (**2a**−**e**, Scheme 7). The triflate salts of **2a** and **2b** were isolated and characterized spectroscopically as well as by elemental analysis and X-ray crystallography; **2c**−**e** were characterized by ^{1}H NMR spectroscopy after in situ protonation of **1c**−**e** with HBF_4·Et_2O in acetonitrile-d_3. The C_{2v} symmetry of the precursors **1a**−**e** was clearly broken as evidenced by the two sets of signals arising from the two halves of the diimine ligands. The coordinated acetonitrile ligands in the isolated compounds **2a** and **2b** were seen as singlets at δ 2.20 and 2.24, respectively, and did not exhibit ^4J(^{195}Pt−H) couplings. On the other hand, broadened (see discussion of π-benzene complexes below) ^4J(^{195}Pt−H) satellites (J = 11−13 Hz) were seen for at least one of the signals arising from the methyl groups at the diimine backbone of **2**. We surmise that the Pt(II) species **2** are produced by protonation at Pt or the phenyl ligand to furnish intermediates that undergo a subsequent elimination of benzene. It has been demonstrated that protonation occurs at Pt for (N−N)PtMe_2 complexes,[60] but it has not been ascertained whether the kinetically preferred site of protonation is at Pt or Ph in (N−N)PtPh_2 complexes. Quantitative production of benzene was seen when the protonation reactions were monitored in NMR tubes.

Scheme 7

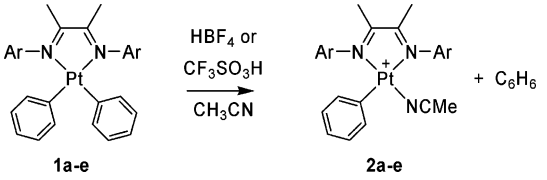

Scheme 8

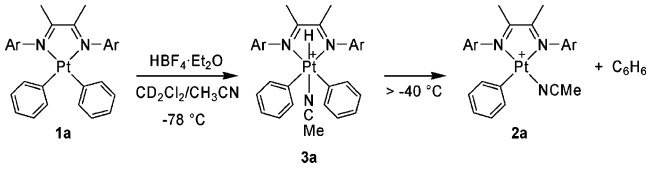

B. Low-Temperature Protonation in the Presence of Acetonitrile. In situ protonation in NMR tubes at −78 °C (see Experimental Section) was performed with HBF_4·Et_2O in order to facilitate the observation of possible intermediates. Protonation of **1a** in CD_2Cl_2 in the presence of acetonitrile led to the immediate formation of the hexacoordinated Pt(IV) hydride (N−N)PtPh_2(H)(NCMe)$^+$ (**3a**) (Scheme 8). The ^{1}H NMR spectrum of **3a** indicated that the two halves of the diimine ligands were symmetry equivalent; from this, we infer that the hydride and MeCN ligands occupy the apical coordination sites. As is commonly seen, Pt(IV) hydrides require stabilization[61] by an additional axial ligand, in our case, acetonitrile. When the NMR sample was heated, **3a** underwent gradual elimination of benzene starting at ca. −40 °C to furnish the Pt(II) solvento complex **2a**. The Pt(IV) hydride exhibited a characteristic Pt-*H* resonance at δ −21.47 with the expected ^{195}Pt satellites, ^1J(^{195}Pt−H) = 1597 Hz. These data agree well with similar data for (N−N)-PtMe_2(H)(X) species.[60,62,63] The coordinated MeCN ligand gave rise to a singlet at δ 3.59, with no discernible Pt−H couplings. The formation of **3a** is consistent with protonation at Pt to give a coordinately unsaturated five-coordinate Pt(IV) hydride that

(54) Perrin, C. L.; Dwyer, T. J. *Chem. Rev.* **1990**, *90*, 935−967.
(55) Carbó, J. J.; Eisenstein, O.; Higgitt, C. L.; Klahn, A. H.; Maseras, F.; Oelckers, B.; Perutz, R. N. *J. Chem. Soc., Dalton Trans.* **2001**, 1452−1461.
(56) Chan, D.; Duckett, S. B.; Heath, S. L.; Khazal, I. G.; Perutz, R. N.; Sabo-Etienne, S.; Timmins, P. L. *Organometallics* **2004**, *23*, 5744−5756.
(57) Orrell, K. G.; Osborne, A. G.; Sik, V.; Da Silva, M. W.; Hursthouse, M. B.; Hibbs, D. E.; Abdul Malik, K. M.; Vassilev, N. G. *J. Organomet. Chem.* **1998**, *555*, 35−47.
(58) Morran, P. D.; Duckett, S. B.; Howe, P. R.; McGrady, J. E.; Colebrooke, S. A.; Eisenberg, R.; Partridge, M. G.; Lohman, J. A. B. *J. Chem. Soc., Dalton Trans.* **1999**, 3949−3960.
(59) Hayes, P. G.; Piers, W. E.; Parvez, M. *Organometallics* **2005**, *24*, 1173−1183.
(60) Wik, B. J.; Lersch, M.; Tilset, M. *J. Am. Chem. Soc.* **2002**, *124*, 12116−12117.
(61) Puddephatt, R. J. *Coord. Chem. Rev.* **2001**, *219*−*221*, 157−185.
(62) Heiberg, H.; Johansson, L.; Gropen, O.; Ryan, O. B.; Swang, O.; Tilset, M. *J. Am. Chem. Soc.* **2000**, *122*, 10831−10845.
(63) Tilset, M.; Johansson, L.; Lersch, M.; Wik, B. J. *ACS Symposium Series 885*; American Chemical Society: Washington, DC, 2004; pp 264−282.

Scheme 9

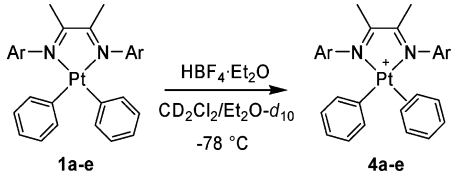

is trapped by acetonitrile. However, kinetically preferred protonation at a phenyl ligand followed by rapid Ph-H oxidative cleavage and subsequent trapping cannot be ruled out.

C. Low-Temperature Protonation in the Absence of Acetonitrile. These protonations were performed in CD_2Cl_2 in the presence of Et_2O-d_{10}, where the latter helps improve the solubility of HBF_4·Et_2O in CD_2Cl_2 at the low temperatures and prevents excessively high local acid concentrations prior to reactant mixing (see Experimental Section). We have no evidence that the ether cosolvent interacts with the resulting Pt π-benzene complexes or perturbs the NMR spectra in any way. The presence of THF, a better donor than Et_2O, results in species with identical chemical shifts and qualitatively the same stability as does the presence of Et_2O.

The low-temperature (−78 °C) protonation of **1a**−**e** under these conditions led to the immediate and quantitative formation of the η^2-coordinated π-benzene complexes (N−N)Pt(C_6H_5)-(π-C_6H_6)$^+$ (**4a**−**e**, Scheme 9), which can only be characterized in situ at sub-ambient temperatures due to onset of benzene elimination at elevated temperatures. The ^{1}H NMR spectra of these complexes exhibit a characteristic singlet arising from the π-C_6H_6 ligand. The signal at ca. δ 6.85−6.97 had a somewhat broadened base; the signal sharpens at higher temperatures, such that the expected $^2J(^{195}Pt-H)$ satellites appear and confirm that the broadening arises from chemical shift anisotropy effects.[64−68] Similar NMR behavior was seen for the (N−N)Pt(Me)-(π-C_6H_6)$^+$ complex that resulted from protonation of (N−N)-Pt(Me)(Ph) (N−N with 2,6-$Me_2C_6H_3$ aryl groups, series "**a**" in this work).[28] The symmetry breaking of the diimine ligand is apparent in the ^{1}H NMR spectra of the π-benzene complexes. All π-benzene complexes **4a**−**e** reacted by benzene liberation when the NMR sample was heated. It was seen that **4a**−**c** slowly eliminated benzene at ca. 0 °C, whereas **4d**−**e** furnished benzene even below −30 °C. The benzene formation occurred with concomitant appearance of the ^{1}H NMR signature of (N−N)-Pt(Ph)(L)$^+$ species, where L may be a solvent molecule. Addition of acetonitrile to the solution after complete benzene elimination led to essentially quantitative generation of the Pt(II) solvento species (N−N)Pt(Ph)(NCMe)$^+$ (done for **2a** and **2b**).

III. X-ray Crystal Structure Determinations of 1a, 1b, 1d, 2a, and 2b. Crystals of **1a**, **1b**, **1d**, **2a**, and **2b** were subjected to structure determinations by X-ray crystallography. Crystallographic data are listed in Table 1. Selected bond distances and angles are summarized in Table 2. Figure 1 shows ORTEP drawings of the five solid-state structures.

All structurally characterized compounds show the expected square-planar environment around Pt(II). The deviations from the least squares planes defined by the central Pt atom and the four Pt-bonded atoms are in the range of 0.005−0.052 Å for Pt and 0.010−0.064 Å for the attached C or N atoms (further details on the metric parameters can be found in the electronic Supporting Information). The sum of the four cis L−Pt−L′ angles around platinum is 360 ± 0.1° for all compounds. In compounds **2a** and **2b**, the Pt−N1 bond trans to the acetonitrile is slightly shorter (0.07−0.08 Å) than the Pt−N2 bond trans to the phenyl ligand, in accordance with a greater trans influence of phenyl versus acetonitrile ligands. There are no significant differences in the Pt−N(diimine) and Pt−C(phenyl) bond distances in **1a** and **1b**. The corresponding bonds in **1d** appear to be slightly elongated in comparison. An expected slight shortening of the Pt−N(diimine) bond distances is seen in the cationic complexes **2a** and **2b** (average value 2.0531 Å) compared to those of the neutral **1a** and **1b** (average 2.112 Å); in view of the mentioned trans influence, this change is most pronounced for the Pt−N1 bond trans to the acetonitrile ligand. The Pt−C(phenyl) bond distances are less affected by the introduction of the positive charge. The N1−Pt−N2 angles are compressed, as is typical for square-planar Pt(II) diimine complexes, from the ideal 90° to an average of 76.56 ± 1.06°. The phenyl ligands and the N-aryl groups of the diimines are twisted away from planarity with the Pt coordination plane, as inferred from the torsion angles at the bottom of Table 2. The aryl groups are twisted out of the coordination plane by 79−88° in **1a**, **1b**, **2a**, and **2b**, all of which are 2,6-dimethyl-substituted at the aryl. In the 3,5-dimethyl-substituted complex **1d**, this torsion angle is considerably smaller, 66−71°. This difference reflects the increased steric demands of the 2,6-dimethyl-substituted systems. Similar trends in dihedral angles are seen in previously published structures of *N*,*N*′-diaryl-substituted (N−N)PtX_2 complexes, with or without 2,6-substituents at the aryl rings.[31,34,35,69−76] On the other hand, the torsion angles of the phenyl groups with respect to the coordination plane span a greater range (48−68° in the neutral 2,6-dimethyl-substituted complexes and 66−85° in the 3,5-dimethyl-substituted one) regardless of the substitution pattern. This suggests that the phenyl ligands have reasonable rotational freedom in *both* ligand environments.

The essentially perpendicular orientation of the 2,6-dimethyl-substituted N-aryl groups with respect to the coordination plane causes the methyl groups to sterically block the access to Pt from above and below the coordination plane. This has a pronounced effect on the stabilities of the Pt(II) π-benzene complexes (vide infra). As a presumably minor effect, one would also expect that this N-aryl rotation serves to attenuate an eventual π-component of substituent electronic effects between the diimine N-aryl groups and the Pt center.

(64) Lallemand, J. Y.; Soulie, J.; Chottard, J. C. *J. Chem. Soc., Chem. Commun.* **1980**, 436−438.
(65) Pregosin, P. S. *Coord. Chem. Rev.* **1982**, *44*, 247−291.
(66) Dechter, J. J.; Kowalewski, J. *J. Magn. Reson.* **1984**, *59*, 146−149.
(67) Anklin, C. G.; Pregosin, P. S. *Magn. Reson. Chem.* **1985**, *23*, 671−675.
(68) Skvortsov, A. N. *Russ. J. Gen. Chem.* **2000**, *70*, 1023−1027.
(69) Johansson, L.; Ryan, O. B.; Rømming, C.; Tilset, M. *Organometallics* **1998**, *17*, 3957−3966.
(70) Yang, K.; Lachicotte, R. J.; Eisenberg, R. *Organometallics* **1998**, *17*, 5102−5113.
(71) Hughes, R. P.; Ward, A. J.; Rheingold, A. L.; Zakharov, L. N. *Can. J. Chem.* **2003**, *81*, 1270−1279.
(72) Yang, K.; Lachicotte, R. J.; Eisenberg, R. *Organometallics* **1997**, *16*, 5234−5243.
(73) Albietz, P. J., Jr.; Yang, K.; Eisenberg, R. *Organometallics* **1999**, *18*, 2747−2749.
(74) Fusto, M.; Giordano, F.; Orabona, I.; Ruffo, F.; Panunzi, A. *Organometallics* **1997**, *16*, 5981−5987.
(75) Ganis, P.; Orabona, I.; Ruffo, F.; Vitagliano, A. *Organometallics* **1998**, *17*, 2646−2650.
(76) Vyater, A.; Wagner, C.; Merzweiler, K.; Steinborn, D. *Organometallics* **2002**, *21*, 4369−4376.

Table 1. Crystallographic Data for **1a**, **1b**, **1d**, **2a**, and **2b**

compound	1a	1b	1d	2a	2b
formula	$C_{32}H_{34}N_2Pt$	$2(C_{34}H_{38}N_2Pt)\cdot CH_2Cl_2$	$C_{32}H_{34}N_2Pt\cdot CH_2Cl_2$	$C_{28}H_{32}N_3Pt\cdot CF_3SO_3$	$C_{30}H_{36}N_3Pt\cdot CF_3SO_3$
formula weight	641.73	1424.49	726.66	754.74	782.80
crystal system	monoclinic	monoclinic	orthorhombic	orthorhombic	monoclinic
color	red	red	red	orange	red
space group	$P2_1/c$	$P2_1/c$	*Pbca*	*Fdd*2	$P2_1/c$
a/Å	11.0148(5)	16.463(3)	17.091(2)	18.344(7)	12.6024(15)
b/Å	14.1617(6)	21.110(2)	16.3830(19)	45.211(11)	22.658(3)
c/Å	17.5859(8)	18.285(4)	22.603(3)	14.761(7)	12.0934(14)
α/°	90	90	90	90	90
β/°	94.5940(10)	94.980(18)	90	90	110.947(2)
γ/°	90	90	90	90	90
V/Å^3	2734.4(2)	6330.7(20)	6328.8(13)	12242(8)	3225.0(7)
Z	4	4	8	16	4
T/K	105	105	105	105	105
F(000)	1272	2840	2880	5952	1552
radiation	Mo Kα (0.71073 Å)	Mo Kα (0.71073 Å)	Mo Kα (0.71073 Å)	Mo Kα (0.71073 Å)	Mo Kα (0.71073 Å)
θ range (°)	1.85 to 28.3	1.86 to 28.33	1.8 to 28.34	1.83 to 28.32	1.73 to 28.32
reflections measured	25106	55804	53545	24816	29556
unique reflections	6565	15104	7559	7123	7768
No. of data/restraint/param.	5772/0/316	8592/0/694	4312/0/343	6542/104/362	6170/0/379
goodness of fit, *F*	1.0464	1.0507	0.9952	1.0599	1.1097
R_1, wR_2 [$I > 3\sigma(I)$]	0.0152, 0.0187	0.0292, 0.0316	0.0327, 0.0375	0.0241, 0.0311	0.0181, 0.0205
largest diff. peak (e Å^{-3})	0.69 to −0.99	2.12 to −1.43	1.43 to −1.56	0.95 to −1.39	1.24 to −1.11

Table 2. Selected Bond Distances and Angles

compound	1a	1b	1d	2a	2b
			Bond distances		
Pt1−N1	2.1036(13)	2.104(4)	2.128(5)	2.017(4)	2.0158(19)
Pt1−N2	2.1050(13)	2.099(4)	2.130(5)	2.079(3)	2.0984(18)
Pt1−N3	−	−	−	1.977(3)	1.971(2)
Pt1−C25	2.0056(16)	2.013(5)	2.033(6)	2.016(5)	2.030(2)
Pt1−C31	2.0150(16)	2.012(5)	2.023(6)	−	−
N1−C1	1.290(2)	1.296(6)	1.301(8)	1.306(5)	1.298(3)
N2−C2	1.295(2)	1.287(6)	1.313(7)	1.288(5)	1.284(3)
C1−C2	1.488(2)	1.489(7)	1.518(8)	1.501(6)	1.491(3)
			Bond angles		
N1−Pt1−N2	75.47(5)	76.11(16)	75.88(18)	77.96(15)	77.47(7)
N1−Pt1−C25	95.04(6)	98.11(17)	97.5(2)	99.91(14)	99.00(8)
N2−Pt1−N3	−	−	−	94.68(15)	95.32(7)
N2−Pt1−C31	99.26(6)	96.27(19)	99.2(2)	−	−
N3−Pt1−C25	−	−	−	87.32(14)	88.26(9)
C25−Pt1−C31	90.25(6)	89.5(2)	87.4(2)	−	−
Pt1−N1−C5	123.08(10)	123.3(3)	120.1(4)	123.9(3)	124.15(14)
Pt1−N2−C14	123.41(10)	123.3(3)	122.3(3)	122.0(3)	123.46(14)
			Torsion angles		
C1−N1−C5−C6	101.0	101.4	71.1	91.5	86.3
C2−N2−C14−C15	−92.1	−82.8	−114.1	−99.6	−85.1
C26−C25−Pt1−N1	102.6	102.7	67.4	62.6	48.0
C32−C31−Pt1−N2	−112.1	−58.9	−85.1	−	−

IV. ^{1}H NMR Spectroscopy of π-Benzene Complexes 4a−c. A. One-Dimensional ^{1}H NMR Spectrum of 4a. The dynamics of the more stable Pt(II) π-benzene complexes **4a−c** will be described in detail in the following, and in order to facilitate the discussion, the NMR spectra of **4a** as a typical example will be discussed in more detail. The standard one-dimensional NMR spectrum of **4a** is shown in Figure 2. The well-resolved spectrum clearly depicts the A_2B patterns of the diimine aryl-H signals, centered at ca. δ 7.25 and 6.70 for the two halves of the molecule. The signal arising from π-benzene is a prominent peak at δ 6.87, whereas the Pt−phenyl group gives rise to the resonances centered at ca. δ 6.20, nicely resolved to show the ortho (δ 6.21), meta (6.15), and para (6.25) hydrogens. These Pt−Ph resonances are located at an unusually high field, especially considering that the complex bears a positive charge. In comparison, the neutral (N−N)$PtPh_2$ compounds **1** show Pt−Ph signals in the range of δ 6.41−6.88; the Pt−Ph of the cationic Pt(II) species **2** (N−N)Pt(Ph)$(NCMe)^+$ resonate at δ 6.58−6.75, the cationic Pt(IV) species **3** (N−N)-$PtPh_2(H)(NCMe)^+$ at δ 6.54−6.94, and the neutral (N−N)Pt-(Me)(Ph)[28] at δ 6.44−6.72. We surmise that the high-field shifts of Pt−Ph in **4a** are caused by aromatic ring current effects that are induced by the neighboring π-benzene ligand. A similar, but even more pronounced, high-field shift was seen for the same reason in the Pt−Me resonance (δ −1.59 at −69 °C) of (N−N)Pt(Me)$(C_6H_6)^+$.[28] The NMR features of **4b** and **4c** were quite similar.

The EXSY spectrum of **4a** (vide infra), if plotted with greater sensitivity than that used for Figure 4, also shows faint NOESY correlations, distinguished by their opposite phase relative to

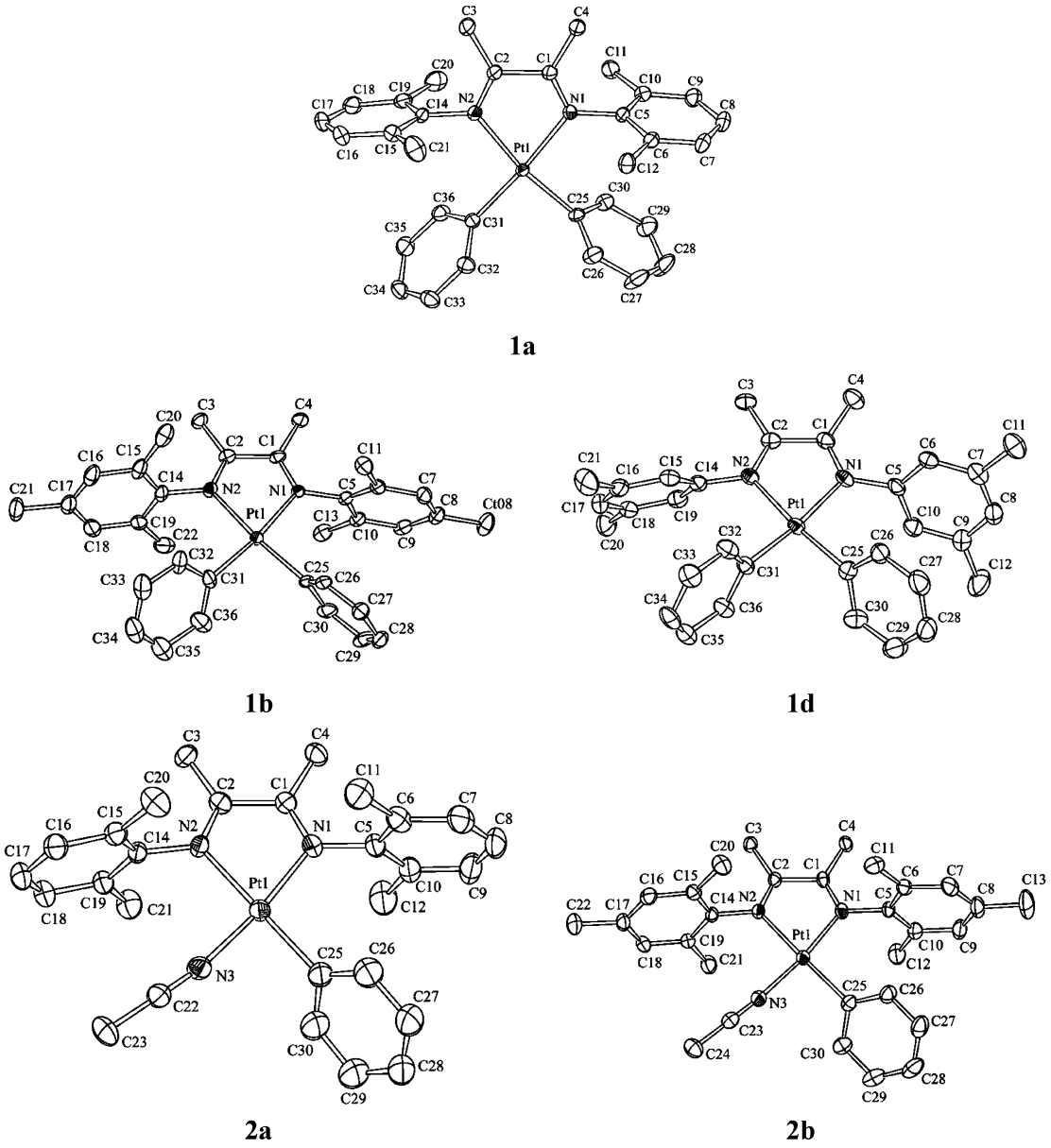

Figure 1. ORTEP drawings of the neutral Pt(II) complexes **1a**, **1b**, and **1d**, and the cationic Pt(II) complexes **2a** and **2b**.

the EXSY cross-peaks, that allows a complete assignment of the aromatic signals. There is a clear NOESY correlation between the π-benzene signal **b** in Figure 2 and a methyl signal at δ 2.44, which correlates with the diimine aryl meta-H at δ 7.30 (which again correlates with the para-H at δ 7.20 in signal group **a**). Conversely, a NOESY cross-peak is seen between the Pt−phenyl meta-H (group **d**) and a methyl signal at δ 2.12, which again correlates with the diimine aryl meta-H at δ 6.70 (which again correlates with the para-H at δ 6.75 in signal group **c**). Thus, the low-field aryl signals **a** centered at δ 7.25 arise from the diimine aryl group that is adjacent to the π-benzene ligand, whereas the low-field signals **c** centered at 6.70 arise from the aryl group that is adjacent to the Pt−phenyl ligand.

B. ^{1}H NMR Spin-Saturation Transfer (SST) for 4a−c. The spectrum in Figure 2 shows no hint of dynamic behavior. Indeed, significant line broadening effects that could be attributed to dynamic phenomena could not be seen at temperatures up to 0 °C, at which sample decomposition by benzene elimination started to dominate. We therefore resorted to the use of spin-saturation transfer (SST) to probe for dynamic processes. The SST technique has been successfully applied to investigate dynamic processes in Tp′Pt systems and to obtain kinetic data for their exchange processes.[51,52] Indeed, we find that irradiation of the π-benzene signal of **4a** leads to a decrease in the intensities of all Pt−Ph signals (Figure 3). However, the effects are modest. Attempts at extracting kinetic parameters were effectively thwarted by insufficient rates of exchange at lower temperatures and competing sample decomposition and benzene elimination, resulting in more complicated spectra less amenable to detailed study at higher temperatures. As a result, extracted rate constants and other kinetic parameters were not very reproducible. This unfortunate situation applied to all three species **4a**−**c**. It should be noted, however, that at optimal temperatures (compromise between desired high rate of exchange and slow rate of sample decomposition) the extracted rate constants from SST measurements agreed to within better than a factor of 2 with those obtained from EXSY spectra (vide infra).

Scheme 10

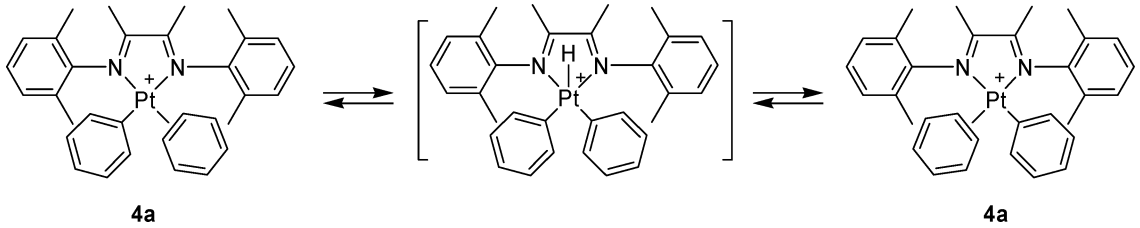

The SST experiment results clearly demonstrated that benzene-H/phenyl-H exchange does occur between protons on the Pt−Ph group and the Pt−(π-benzene) ligand. The most reasonable mechanistic scenario for this exchange process is the interconversion that occurs by oxidative cleavage of a C−H bond in the π-benzene complex, leading to a Pt(IV) hydridodiphenyl intermediate (Scheme 10), which may or may not bear a second, weakly coordinated yet stabilizing, axial ligand. The scenario depicted in Scheme 10 reveals that benzene-H/phenyl-H exchange via this mechanism leads to a symmetrization of the system since in the Pt(IV) intermediate the left and right halves of the molecule are symmetry equivalent. Thus, dynamic NMR should demonstrate not only equilibration of phenyl and benzene protons but also a "side-shift" of the diimine ligand moiety. This behavior is described in the following paragraphs.

C. Qualitative ^{1}H NMR EXSY Spectroscopy of 4a−c and 4e. Two-dimensional ^{1}H−^{1}H EXSY spectroscopy was performed as detailed in the Experimental Section. A typical sample EXSY spectrum of **4a** is shown in Figure 4. The EXSY spectrum clearly shows correlation cross-peaks between the π-benzene and all positions of the Pt−phenyl group (**A**). Qualitatively, it appears that the cross-peak intensities for the three phenyl positions roughly decrease in the order ortho, meta > para, which may simply reflect the expected 2:2:1 ratio that would result in the event of a rapidly rotating π-benzene ring. There are no well-resolved EXSY correlations internally between the positions of the phenyl group. The symmetrization suggested by Scheme 10 is clearly evidenced by correlation cross-peaks between the hydrogen atoms in the 3,5-positions (**B**) of the aryl groups at each half of the diimine ligand, as well as between the two 4-positions (**C**). In addition, the symmetrization is corroborated (not shown in Figure 4) by correlation cross-peaks between the methyl groups at the aryl rings and between the methyl groups at the diimine backbone of the left- and right-hand halves of the ligand. Entirely analogous behavior was demonstrated for compounds **4b** and **4c**.

Compound **4e** was also subjected to an EXSY spectroscopy investigation. Faint exchange cross-peaks could be seen in the 2D EXSY spectra at −33 °C, but sample decomposition with benzene release commenced already at this temperature and it was not possible to investigate this compound in more detail. Thus, in qualitative terms, it appears that the exchange processes in **4a**−**c** must be very rapid compared to the rate of benzene elimination, whereas benzene elimination, relatively speaking, is much faster for **4e**.

D. Kinetics of Exchange Processes by EXSY Spectroscopy. The kinetics of the exchange processes in **4a**−**c** were investigated over the approximate temperature range of −50 to −15 °C. The temperature interval was limited individually for each complex by exchange kinetics being too slow to be reliably measured on the low-temperature side, and by complications due to sample decomposition and benzene release on the high-temperature side. In addition to **4a**−**c**, the deuterated species **4a**-d_{10} was prepared by protonation of **1a**-d_{10} in order to estimate H/D kinetic isotope effects, if any, on the exchange process. It is worth noting that the comparison of **4a** and **4a**-d_{10} is based on the exchange rates that are inferred from the symmetrization of the diimine ligand resonances. The exchange kinetics are obtained from observing the *same exchanging nuclei* using exactly the *same method* for both species, hopefully reducing potential errors that might be introduced by utilizing different methods for the isotopomers. The basis for the extraction of kinetic data produced by the EXSY experiments is integration

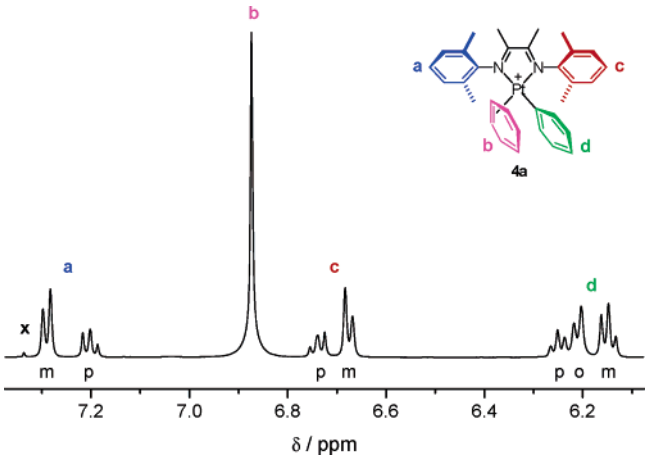

Figure 2. Aromatic region of the ^{1}H NMR spectrum (CD_2Cl_2, 300 MHz, −23 °C) of **4a**(BF_4). a: Aryl protons. b: π-Benzene (shoulders originating from ^{195}Pt satellites, broadened by chemical shift anisotropy, are clearly discernible only above ca. 0 °C; spectra of **4a** alone are not available at these temperatures because of the accompanying decomposition of **4a**). c: Aryl protons. d: Phenyl protons. x: Uncoordinated benzene.

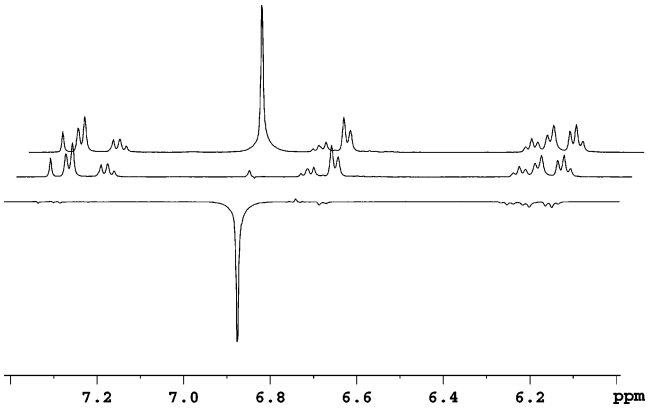

Figure 3. Stacked plot of a spin-saturation transfer experiment of **4a** depicting, from top to bottom, the normal ^{1}H NMR spectrum (CD_2Cl_2, 500 MHz, 250 K), the irradiated (on π-benzene) spectrum, and the difference spectrum.

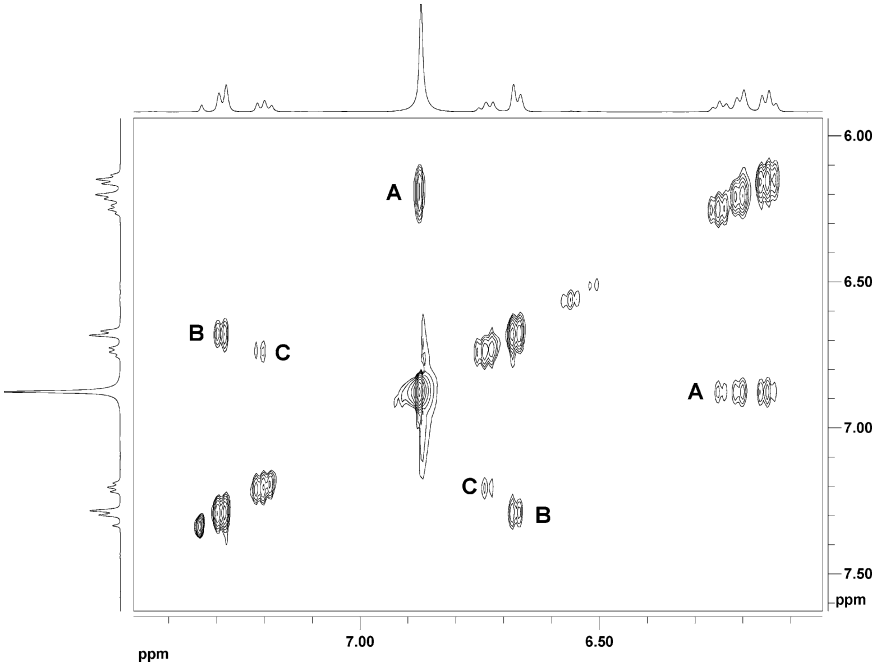

Figure 4. EXSY ^{1}H NMR spectrum of **4a** (−23 °C, mixing delay time 0.96 s, 384 increments in *F*1 direction and 16 transients per increment. **A**: Cross-peaks arising from π-benzene to phenyl exchange. **B** and **C**: Cross-peaks caused by the diimine ligand side-shift exchange (symmetrization). Free benzene appears as a minor peak at 7.33. No negative phase (NOESY) peaks are discernible at the sensitivity used in this spectrum.

of the cross-peak volumes in the EXSY NMR spectra.[54] In order for EXSY to serve the purpose, exchange must be slow enough that the exchanging signals are resolved and fast enough that the memory of spin exchange is not removed by relaxation processes. The available exchange rate window is typically ca. 10^{-2} to 10^2 s^{-1}.[77] For consistency, *all kinetic data reported herein were extracted by integration of the cross-peaks in the aromatic region arising from the symmetrization of the aryl hydrogens of the diimine ligand* (**B** and **C** in Figure 4). These signals were well separated from all other signals for **4a**−**c** and could be easily integrated. The results were compared in some instances by integration of the cross-peaks from the interchanging methyl groups at the diimine backbone or at the diimine aryl groups when these were well resolved, and this procedure gave rate constants that were identical within experimental uncertainties to those obtained on the basis of the aromatic region. In addition, the data were further checked by integration of the phenyl/π-benzene cross-peaks (**A** in Figure 4) for **4a**, which also led to the same quantitative results. However, data extracted from these cross-peaks might be somewhat perturbed for reasons given in the following. First, there is a potential for NOESY interactions between hydrogens at the phenyl and π-benzene groups (most likely a small, if not negligible, effect due to on the average rather large H−H distances); the opposite sign of the NOESY cross-peaks relative to the EXSY ones[78] will in this case lead to an underestimation of the EXSY cross-peak intensities and the subsequently derived exchange rate constants. Second, unless the rate of rotation of the π-benzene ring (for which we have no data) is very fast relative to the exchange rate, the rates of exchange into the ortho, meta, and para positions of the phenyl ring may be somewhat different. This may cause some uncertainties in the derived rate data because the kinetics of the positional migration of Pt with respect to the face of the π-benzene ring will be involved. Nevertheless, rate constants that were derived from the phenyl/π-benzene cross-peaks were essentially indistinguishable from those obtained from the diimine symmetrization cross-peaks. This establishes without doubt that the two spectroscopically observed exchange phenomena, symmetrization and phenyl/π-benzene exchange, arise from the same dynamic process. The Eyring equation was applied on the *k* versus *T* data for compounds **4a**−**c** and **4a-*d*$_{10}$** and provided the kinetic parameters that are summarized in Table 3. The corresponding Eyring plots, all linear in the available temperature ranges, are depicted in Figure 5.

Table 3. Kinetic Parameters for the Exchange Processes of **4a**−**c** as Determined by Quantitative EXSY ^{1}H NMR Spectroscopy[a]

compound	*T* range (°C)	$\Delta H^{\ddagger}$ (kJ mol^{-1})	$\Delta S^{\ddagger}$ (J K^{-1} mol^{-1})	*k* (0 °C)[b] (s^{-1})
4a	−49 to −19	70.2 (3.6)	37 (15)	18.3
4a-*d*$_{10}$	−34 to −19	79.6 (8.1)	58 (33)	3.6
4b	−44 to −14	70.9 (3.7)	38 (15)	15.4
4c	−49 to −24	71.9 (4.6)	48 (19)	34.2

[a] $\Delta H^{\ddagger}$ and $\Delta S^{\ddagger}$ were estimated from a linear regression analysis of *k* versus 1/*T* data. The uncertainties given were obtained from a nonlinear least-squares analysis as described by Girolami and co-workers,[79] assuming an uncertainty in *T* of 1 K and in *k* of 5% of its numerical value. [b] By extrapolation of the Eyring plot using the calculated $\Delta H^{\ddagger}$ and $\Delta S^{\ddagger}$ data.

It has been pointed out that exchange rate constants obtained by dynamic NMR methods often differ from those of the actual chemical exchange, *k*.[21,80,81] This occurs because a fraction of the chemical process will occur without observable magnetization transfer. As recently discussed, for a symmetrical exchange

(77) Claridge, T. D. W. *High-Resolution NMR Techniques in Organic Chemistry*; Pergamon: Amsterdam, 1999; Tetrahedron Organic Chemistry Series Vol. 19.

(78) The sign of NOESY peaks may change at the low temperatures when the slow tumbling regime is reached. The NOESY signs were not further investigated since the quantitative kinetic data are derived from the diimine symmetrization rather than the phenyl/π-benzene cross-peaks and therefore should not be perturbed by NOESY contributions.

(79) Morse, P. M.; Spencer, M. D.; Wilson, S. R.; Girolami, G. S. *Organometallics* **1994**, *13*, 1646−1655.

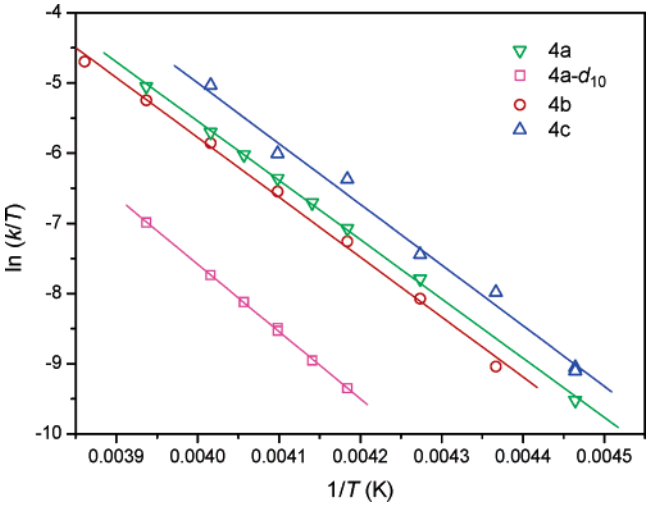

Figure 5. Eyring plot of the kinetic data for the left/right symmetrization process of **4a**−**c** in CD_2Cl_2 containing 1 M (16 vol %) Et_2O-d_{10}.

between two equally populated sites, $k = 2k_{obs}$.[21] In the equation that is applied here (see Experimental Section), given by Perrin and Dwyer,[54] the exchange rate constant for exchange between A and B sites is defined as $k = k_{AB} + k_{BA}$; that is, the factor of 2 has been taken into account and the calculated k data may be directly applied.

Discussion

As discussed in the Introduction, isotopic scrambling has established that exchange of hydrogen atoms between methyl, phenyl, π-benzene, and hydride sites of organometallic complexes is a common phenomenon in systems that are capable of activating C−H bonds. Only rarely have these exchange processes been directly observed by spectroscopic methods, and rate data were in those cases extracted from SST[51,52,82] or line-broadening[83] experiments. In this contribution, we have utilized 2D exchange spectroscopy for the first time to probe the energetics of such processes.

EXSY versus SST. It is apparent from the Results section that we find EXSY to offer great advantages compared to SST experiments. This is in full agreement with experiences made by other groups, although each method has its own advantages.[84−87] In the present case, two important advantages are that (a) better signal separation is achieved in 2D than in 1D, and (b) integration of the well-resolved 2D EXSY spectra could be performed with far better accuracy and improved signal-to-noise ratio compared to the 1D SST. The EXSY spectra give access to quantitative data at slower exchange rates than do the SST measurements; hence, measurements can be conducted at lower temperatures. This is of particular importance when dealing with the thermally sensitive π-benzene complexes investigated herein.

Pt(II) versus Pt(IV) from Protonation of Pt(II). Octahedral Pt(IV) hydrides are frequently generated by protonation of square-planar Pt(II) precursors and are usually quite unstable unless they have a strongly bonded ligand in the other apical position trans to the hydride.[61] Thermally very robust species can result if this site is occupied by a tridentate chelate, quite notably derivatives of hydridotris(pyrazolyl)borate[88−91] or triazacyclononane.[92−94] Complexes that bear a nonchelating apical ligand tend to be considerably less stable. Temperatures that facilitate the (relatively speaking) high-energy ligand dissociation usually initiate reductive elimination processes, which in general proceed at greater ease from five-coordinate Pt(IV) than from the six-coordinate precursors. It is interesting that the π-benzene complex **4a** is thermally more robust in the absence of acetonitrile than is the Pt(IV) hydridodiphenyl complex **3a** in the presence of acetonitrile. Whereas **4a** eliminates benzene at ca. 0 °C, **3a** undergoes benzene elimination at −30 °C without observation of the more robust **4a** as an intermediate. It is nevertheless likely that the π-benzene complex is an intermediate in the elimination of benzene from **3a**. The reason for this is that, on the basis of the current understanding of the mechanism of benzene C−H activation at (N−N)Pt(Me)-$(H_2O)^+$ complexes, hydrocarbon elimination is an *associative* process. Acetonitrile dissociation from **3a** is expected to have a reasonably high activation barrier. We have recently determined that methane elimination from (N−N)$Pt(Me)_2$(H)-$(NCMe)^+$ proceeds with rate-limiting acetonitrile dissociation with $\Delta H^{\ddagger}$ ca. 80 kJ mol^{-1}.[95] A range of H/D isotope and aryl positional scrambling experiments suggests that the ensuing C−H reductive coupling which produces the π-benzene intermediate will proceed with a relatively low activation barrier. The final step in the reductive elimination, benzene loss from the cationic π-benzene complex, is expected to occur associatively, and this will be a relatively facile process in the presence of acetonitrile. The overall process is depicted in Scheme 11.

This scenario agrees to a great extent with recent findings by Templeton and co-workers.[53] Protonation of (κ^3-Tp′)PtH_2-Ph at −78 °C furnishes the Pt(II) π-benzene complex (κ^2-HTp′)-Pt(H)(η^2-C_6H_6)$^+$ (formally neutral at Pt since the positive charge resides at a protonated N of a pendant pyrazole ring), which is stable at low temperatures. In the presence of acetonitrile, this π-benzene complex exists in equilibrium (quantified from −80 to −30 °C) with the Pt(IV) phenyl complex (κ^2-HTp′)$Pt(H)_2$-(Ph)$(NCMe)^+$ (also neutral at Pt) until benzene loss commences above −30 °C. We suspect that the reason that Pt(II) and Pt(IV) coexist in this case but not in our system may be due to a relative strengthening of the Pt−NCMe, compared to the Pt−(π-C_6H_6) bond in our cationic-at-Pt complexes. Accordingly, (N−N)Pt-(Ph)(η^2-C_6H_6)$^+$ complexes are not seen in the presence of acetonitrile, but can be observed in the less nucleophilic medium

(80) Mann, B. E. *J. Chem. Soc., Perkin Trans. 2* **1977**, 84−87.
(81) Green, M. L. H.; Wong, L. L.; Sella, A. *Organometallics* **1992**, *11*, 2660−2668.
(82) Rybtchinski, B.; Konstantinovsky, L.; Shimon, L. J. W.; Vigalok, A.; Milstein, D. *Chem.−Eur. J.* **2000**, *6*, 3287−3292.
(83) Gross, C. L.; Girolami, G. S. *J. Am. Chem. Soc.* **1998**, *120*, 6605−6606.
(84) Ming, L. J.; Jang, H. G.; Que, L., Jr. *Inorg. Chem.* **1992**, *31*, 359−364.
(85) Shao, W.; Liu, G.; Tang, W. *J. Inorg. Biochem.* **1995**, *57*, 103−113.
(86) Denkova, P. S.; Dimitrov, V. S. *Magn. Reson. Chem.* **1999**, *37*, 637−646.
(87) Vassilev, N. G.; Dimitrov, V. S. *Magn. Reson. Chem.* **2001**, *39*, 607−614.
(88) Canty, A. J.; Dedieu, A.; Jin, H.; Milet, A.; Richmond, M. K. *Organometallics* **1996**, *15*, 2845−2847.
(89) O'Reilly, S. A.; White, P. S.; Templeton, J. L. *J. Am. Chem. Soc.* **1996**, *118*, 5684−5689.
(90) Haskel, A.; Keinan, E. *Organometallics* **1999**, *18*, 4677−4680.
(91) Reinartz, S.; White, P. S.; Brookhart, M.; Templeton, J. L. *Organometallics* **2000**, *19*, 3748−3750.
(92) Prokopchuk, E. M.; Jenkins, H. A.; Puddephatt, R. J. *Organometallics* **1999**, *18*, 2861−2866.
(93) Prokopchuk, E. M.; Puddephatt, R. J. *Can. J. Chem.* **2003**, *81*, 476−483.
(94) Sobanov, A. A.; Vedernikov, A. N.; Dyuker, G.; Solomonov, B. N. *Russ. J. Gen. Chem.* **2003**, *73*, 842−846.
(95) Reductive elimination of methane from an (N−N)$PtMe_2$(NCMe)H^+ (N−N ligand as in the "a" series of this work) complex occurs with rate-limiting MeCN dissociation with an activation enthalpy of ca. 80 kJ mol^{-1}. Wik, B. J.; Tilset, M.; van Eldik, R.; Ivanoviç-Burmazoviç, I. *Inorg. Chem.* Submitted for publication.

Scheme 11

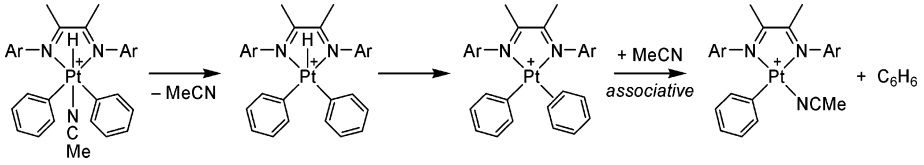

of this investigation (dichloromethane with small quantities of diethyl ether).

Ligand Effects on Stabilities of π-Benzene Complexes. All (N−N)$PtPh_2$ complexes described herein give observable π-benzene complexes upon protonation at −78 °C in dichloromethane with ether. However, the thermal stabilities of the π-benzene complexes strongly depend on the identity of the N−N ligand system. The species that have 2,6-dimethyl-substituted N-aryl groups at the diimine give rise to the relatively stable π-benzene complexes **4a**−**c** that eliminate benzene only at elevated temperatures (ca. −30 °C), whereas the complexes **4d**−**e** that bear no substituents in the 2,6-positions slowly undergo benzene loss already at −78 °C. This difference in behavior is readily understood in view of the anticipated[28,31,33,48] associative nature of the hydrocarbon elimination. The 2,6-substituents tend to shield the Pt center with respect to attack by an external nucleophile, whatever its identity might be under the reaction conditions (Et_2O, traces of water, counteranion). The steric protection of the Pt center is evidenced by the X-ray crystal structures of **1a** and **1b** as has already been discussed. There are only minor ligand effects on the rates of exchange for the three 2,6-dimethyl sterically protected complexes **1a**−**c**. The steric demands at the metal should be the same for the series. Electronic effects may be anticipated to be modest, in particular, because the aryl rings are twisted out of the coordination plane so as to attenuate any resonance effects. Although the kinetics of benzene loss were not investigated here, it was seen that, at least qualitatively, the benzene loss from **4a-*d*$_{10}$** commenced at the same temperature as for **4a**, indicating only a negligible, if any, H/D isotope effect on the rate of benzene loss from the π-benzene complex.

Kinetics of the Exchange Process. The kinetic data for the exchange processes for **4a**−**c** show activation enthalpies of ca. 70 kJ mol^{-1} and slightly positive (with significant uncertainties) entropies of activation. The enthalpy values may be compared to those reported by Templeton and co-workers[51] for exchange in (κ^2-HTp′)Pt(η^2-C_6H_6)H^+ ($\Delta H^{\ddagger}$ = 49(2) kJ mol^{-1}). The latter is formally neutral at Pt, and the lower barrier may be caused by easier access to the intermediate Pt(IV) dihydridophenyl species starting from a more electron-rich, formally neutral Pt center than from the positively charged Pt centers that we have investigated. Another and more striking difference lies in our observation of quite positive activation entropies; in comparison, the exchange process for (κ^2-HTp′)Pt(η^2-C_6H_6)H^+ exhibited $\Delta S^{\ddagger}$ = −16(8) J K^{-1} mol^{-1}. It is not obvious to us what causes the slightly positive $\Delta S^{\ddagger}$ in our systems. One possibility might be that the putative five-coordinate Pt(IV) hydridodiphenyl species attain a trigonal bipyramidal geometry that allows more rotational freedom in the otherwise sterically encumbered system.

Kinetic Isotope Effects. The kinetic isotope effects (KIEs) were measured on (N−N)Pt(C_6D_5)(C_6D_5H)$^+$ (**4a-*d*$_{10}$**), prepared by protonation of **1a-*d*$_{10}$**. Thus, there is one proton left in the Pt−phenyl and π-benzene moieties of the molecule when the measurements are performed, and (disregarding equilibrium isotope effects, EIEs) this proton will be evenly distributed between these moieties. Thus, the measured isotope effect will be somewhat smaller than what would be seen for a fully deuterated compound **4a-*d*$_{11}$**. Nevertheless, the measured isotope effects are quite large; temperature-dependent KIEs calculated from measured rate constant at identical temperatures (thus minimizing uncertainties in *T*) smoothly decrease from 9.7 ± 1.0 at −34 °C to 6.9 ± 0.7 at −19 °C. Extrapolation using the Eyring activation parameters led to values of 5.1 at 0 °C and 3.6 at 25 °C. These isotope effect values leave little doubt that C−H(D) bond breaking must be involved in the dynamic process.

Our data can be compared with previously reported KIEs for arene C−H activation reactions at "late" transition-metal complexes. The following summary includes KIEs for reactions that occur from preformed η^2-benzene complexes or KIEs for intramolecular competition experiments on partially deuterated benzenes. This way, eventual KIEs or EIEs on the preceding benzene coordination need not be considered—as is also the case for the Pt arene complexes under investigation here. The intramolecular oxidative C−H bond cleavage of benzene exhibited k_H/k_D = 3.0 (−14 °C) for (κ^2-HTp′)Pt(X)(η^2-C_6X_6)$^+$, and 4.7 (−32 °C) for (κ^2-HTp′)Pt(C_6X_5)(η^2-C_6X_6)$^+$ with X = H or D.[52] The photolytically generated TpRe(O)(Cl) fragment exhibited k_H/k_D = 4.0 (ambient temperature) in the intramolecular competition for C−H versus C−D bonds of 1,3,5-$C_6D_3H_3$.[96] Similarly, k_H/k_D = 1.4 (−40 °C) for Cp*Rh(PMe_3),[24] 1.3 (75 °C) for (Me_3tacn)Rh(PMe_3)(H)(Me)$^+$,[97] and 3.2 (110 °C) for (acac)$_2$Ir(Me)(pyr)[98] in reactions with 1,3,5-$C_6D_3H_3$. A rather large k_H/k_D = 20 ± 6 (133 °C) (presented with extreme caution due to experimental ambiguities)[99] was estimated for the reaction of *trans*-(PMe_3)$_2$Pt(CH_2CMe_3)(OTf) with C_6D_5H. For Pt, additional KIE data that pertain to the overall two-step process of benzene coordination and following C−H activation should also be mentioned. For example, k_H/k_D = 3.3 (110 °C) for the thermolysis of (dmpe)Pt(Me)(O_2CCF_3) in C_6H_6 versus C_6D_6.[100] Structurally most relevant to the case at hand, k_H/k_D values of ca. 2 (25 °C) were determined for reactions of (diimine)Pt(H_2O)(CH_3)$^+$ complexes with C_6H_6 versus C_6D_6 when the diimine moiety was sterically relatively unencumbered so that C−H(D) activation rather than benzene coordination was rate limiting.[32] An analogous Pd complex exhibited k_H/k_D = 4.1 at 25 °C.[101] Reactions at closely related Pt complexes with C_6H_6 versus C_6D_6 (45−55 °C) exhibited k_H/k_D = 1.3 for

(96) Brown, S. N.; Myers, A. W.; Fulton, J. R.; Mayer, J. M. *Organometallics* **1998**, *17*, 3364−3374.
(97) Wang, C.; Ziller, J. W.; Flood, T. C. *J. Am. Chem. Soc.* **1995**, *117*, 1647−1648.
(98) Bhalla, G.; Liu, X. Y.; Oxgaard, J.; Goddard, W. A., III; Periana, R. A. *J. Am. Chem. Soc.* **2005**, *127*, 11372−11389.
(99) Brainard, R. L.; Nutt, W. R.; Lee, T. R.; Whitesides, G. M. *Organometallics* **1988**, *7*, 2379−2386.
(100) Peters, R. G.; White, S.; Roddick, D. M. *Organometallics* **1998**, *17*, 4493−4499.

$[Ph_2B(CH_2PPh_2)_2]Pt(Me)(THF)$, 6.5 for $[Ph_2Si(CH_2PPh_2)_2]Pt(Me)(THF)^+$, and ca. 6 for $[H_2C(CH_2PPh_2)_2]Pt(Me)(THF)^+$.[39] With these data as a backdrop, it appears that our measured KIEs are in the normally observed range for benzene C−H(D) activation at transition-metal complexes.

When large KIEs are encountered in C−H versus C−D bond cleavage reactions, possible contributions from tunneling need to be considered. In Bell's model for the reaction rates of isotopic molecules,[102] the observed isotope effect is the product of a semiclassical isotope effect and a tunneling correction. An isotope effect that is larger than that expected from the semiclassical model is explained by tunneling. The importance of the tunneling correction can be inferred from the temperature dependence of the isotope effect. Thus, tunneling may be suggested[102] if the ratio of Arrhenius pre-exponential factors, A_D/A_H, is greater than 1.4, and the difference in activation energies, $E_a^D - E_a^H$, is significantly greater than that calculated from zero-point energy differences (ca. 4.8 kJ mol^{-1} based on typical C−H(D) vibration frequencies). The kinetic data in Table 3 lead to $A_D/A_H = 12.8$ and $E_a^D - E_a^H = 9.4$ kJ/mol, which fulfill both criteria to suggest tunneling. The possibility that tunneling may be involved in C−H activation and related reactions at transition metals has been proposed on the basis of experiments[103−107] and calculations,[108−112] including additions of methane at coordinatively unsaturated Pd^0 centers.

The conventional descriptions of isotope effects are based on estimations of zero-point energy (ZPE) differences between reactants and transition states (KIE) or products (EIE), and the magnitude of the IE is usually interpreted on the basis of ZPE changes in bonds being cleaved or formed during the reaction. More recently, it has been demonstrated that this description is too simplistic for many organometallic systems. In a classical study, Bergman and co-workers determined EIE values as large as ca. 20 (−80 °C) for coordination of cyclohexane versus cyclohexane-d_{12},[113] and ca. 14 (−108 °C) for neopentane versus neopentane-d_{12},[114] at the Cp*Rh(CO) fragment in liquid Kr. These processes involve no C−H(D) bond breaking at all, and it was concluded that vibrational modes other than the C−H(D) bond being broken must make a significant contribution to the zero-point energy of the metal alkane complex.[114] Experimental data in support of this view have also been obtained for reactions at early transition-metal moieties.[115] It is now commonly considered that the detailed interpretation of EIE and KIE data for metal-mediated C−H activation processes and related reactions often necessitates a full statistical mechanical treatment of the isotopic reaction rates or equilibria.[23,115−120] It is evident that great care must be taken not to over-interpret the mechanistic significance of measured isotope effects for multistep, and not even single-step, reaction sequences.[23,121] The source of the rather strongly temperature-dependent KIEs for the dynamic processes in **4a**, whether classical or tunneling in origin, cannot be sorted out without resorting to calculations.

Concluding Remarks

Protonation of $(N-N)PtPh_2$ complexes yields Pt(II) phenyl/π-benzene complexes in noncoordinating solvents and Pt(IV) hydridodiphenyl species in coordinating solvents. The SST and EXSY spectra demonstrate that the Pt(II) species undergo dynamic exchange processes that most likely involve facile C−H bond cleavage reactions that access Pt(IV) hydridodiphenyl intermediates. The kinetics of the oxidative cleavage/reductive coupling of C−H bonds of coordinated arenes in Pt(II) diimine systems have been probed for the first time, and the involvement of C−H bond cleavage reactions was directly demonstrated by the large kinetic isotope effects. It is evident that 2D EXSY spectroscopy offers great advantages over SST. In particular, the greater sensitivity of EXSY allows the reaction dynamics to be investigated at lower temperatures than does SST—of particular importance when dealing with thermally sensitive complexes. We plan to explore other metal-mediated C−H bond cleavage/bond-forming reactions using these methods and will describe the findings in due time.

Experimental Section

General Procedures. Deuterated solvents were used as received without further drying (CD_2Cl_2, Et_2O-d_{10}, CD_3CN, C_6D_6). NMR spectra were recorded on Bruker DPX200, DPX300, and DRX500 instruments. ^{1}H NMR chemical shifts (δ) are reported in parts per million (ppm) relative to TMS using the residual proton resonances of the solvent (δ 5.32 in CD_2Cl_2, 7.15 in C_6D_6, 7.24 in $CDCl_3$). ^{19}F NMR chemical shifts (δ) are reported in ppm relative to $CFCl_3$ (0 ppm). ^{195}Pt NMR chemical shifts (δ) are referenced according to the 2001 IUPAC "unified scale" recommendation[122] with $\Xi = 21.496784$. Elemental analyses were performed by Ilse Beetz Mikroanalytisches Laboratorium, Kronach, Germany. UV−visible spectra were recorded on a Hewlett-Packard 8452A spectrophotometer and are reported as λ_{max} (nm), $\epsilon \times 10^{-3}$ (M^{-1} cm^{-1}). The diimines (diimine = ArN═CMe−CMe═NAr),[32,123,124] $Ph_2Pt(SMe_2)_2$,[125] and $PtCl_2(SMe_2)_2$[126] were prepared as previously published, and the $(diimine)PtPh_2$ complexes were prepared by methods

(101) Ackerman, L. J.; Sadighi, J. P.; Kurtz, D. M.; Labinger, J. A.; Bercaw, J. E. *Organometallics* **2003**, *22*, 3884−3890.
(102) Bell, R. P. *The Proton in Chemistry*; Cornell: Ithaca, NY, 1973; pp 275−285.
(103) Reinaud, O. M.; Theopold, K. H. *J. Am. Chem. Soc.* **1994**, *116*, 6979−6980.
(104) Chowdhury, S.; Banerjee, R. *J. Am. Chem. Soc.* **2000**, *122*, 5417−5418.
(105) Bryant, J. R.; Mayer, J. M. *J. Am. Chem. Soc.* **2003**, *125*, 10351−10361.
(106) Yoder, J. C.; Roth, J. P.; Gussenhoven, E. M.; Larsen, A. S.; Mayer, J. M. *J. Am. Chem. Soc.* **2003**, *125*, 2629−2640.
(107) Cramer, C. J.; Kinsinger, C. R.; Pak, Y. *THEOCHEM* **2003**, *632*, 111−120.
(108) Espinosa-García, J.; Corchado, J. C.; Truhlar, D. G. *J. Am. Chem. Soc.* **1997**, *119*, 9891−9896.
(109) Mamaev, V. M.; Gloriozov, I. P.; Ishchenko, S. Y.; Simonyan, V. V.; Myshakin, E. M.; Prisyajnyuk, A. V.; Ustynyuk, Y. A. *J. Chem. Soc., Faraday Trans.* **1995**, *91*, 3779−3782.
(110) Mamaev, V. M.; Prisyazhnyuk, A. V.; Gloriozov, I. P.; Ischenko, S. Ya.; Ustynyuk, Y.; Alekseiko, L. N. *Kinet. Catal.* **1998**, *39*, 162−166.
(111) Mamaev, V. M.; Gloriozov, I. P.; Simonyan, V. V.; Zernova, E. V.; Myshakin, E. M.; Babin, Y. V. *Mendeleev Commun.* **2000**, 12−14.
(112) Mamaev, V. M.; Gloriozov, I. P.; Simonyan, V. V.; Babin, Y. V.; Lemenovskii, D. A. *Mendeleev Commun.* **2000**, 155−157.
(113) Weiller, B. H.; Wasserman, E. P.; Bergman, R. G.; Moore, C. B.; Pimentel, G. C. *J. Am. Chem. Soc.* **1989**, *111*, 8288−8290.
(114) Bengali, A. A.; Schultz, R. H.; Moore, B.; Bergman, R. G. *J. Am. Chem. Soc.* **1994**, *116*, 9585−9589.
(115) Slaughter, L. M.; Wolczanski, P. T.; Klinckman, T. R.; Cundari, T. R. *J. Am. Chem. Soc.* **2000**, *122*, 7953−7976.
(116) bu-Hasanayn, F.; Krogh-Jespersen, K.; Goldman, A. S. *J. Am. Chem. Soc.* **1993**, *115*, 8019−8023.
(117) Rabinovich, D.; Parkin, G. *J. Am. Chem. Soc.* **1993**, *115*, 353−354.
(118) Hascall, T.; Rabinovich, D.; Murphy, V. J.; Beachy, M. D.; Friesner, R. A.; Parkin, G. *J. Am. Chem. Soc.* **1999**, *121*, 11402−11417.
(119) Bender, B. R. *J. Am. Chem. Soc.* **1995**, *117*, 11239−11246.
(120) Bender, B. R.; Kubas, G. J.; Jones, L. H.; Swanson, B. I.; Eckert, J.; Capps, K. B.; Hoff, C. D. *J. Am. Chem. Soc.* **1997**, *119*, 9179−9190.
(121) Jones, W. D. *Acc. Chem. Res.* **2003**, *36*, 140−146.
(122) Harris, R. K.; Becker, E. D.; Cabral De Menezes, S. M.; Goodfellow, R.; Granger, P. *Pure Appl. Chem.* **2001**, *73*, 1795−1818.
(123) Tom Dieck, H.; Svoboda, M.; Greiser, T. *Z. Naturforsch. B* **1981**, *36B*, 823−832.
(124) Wang, X.; Chakrapani, H.; Madine, J. W.; Keyerleber, M. A.; Widenhoefer, R. A. *J. Org. Chem.* **2002**, *67*, 2778−2788.
(125) Scott, J. D.; Puddephatt, R. J. *Organometallics* **1983**, *2*, 1643−1648.
(126) Hill, G. S.; Irwin, M. J.; Levy, C. J.; Rendina, L. M.; Puddephatt, R. J. *Inorg. Synth.* **1998**, *32*, 149−153.

analogous to that previously published by us.[28] Because of the thermal instability of $Ph_2Pt(SMe_2)_2$, this compound is frequently used without purification. $Ph_2Pt(SMe_2)_2$ is considered as a monomer for convenience, although it is supposed to exist as mixtures of dimers and trimers.[127] Low-temperature protonation experiments in NMR tubes were performed by modifications of the previously reported procedures.[60,63] The temperature calibration for the low-temperature experiments was done using a thermocouple situated inside a thin glass tube that was inserted into an NMR tube with methanol. For NMR assignment, Ph-*H* designates Pt−Ph resonances, whereas Ar-*H* is used for N-aryl proton resonances. Mass spectra were recorded on a Waters Micromass Q-TOF2W instrument.

$(C_6D_5)_2Pt(SMe_2)_2$. To a solution of C_6D_5Br (270 μL, 2.54 mmol) in dry ether (7 mL) cooled at −78 °C was added *n*-BuLi (1.56 mL of a 1.6 M solution in hexanes, 2.54 mmol). The mixture was stirred at −78 °C under N_2 for 15 min and allowed to slowly warm to 25 °C. The mixture was cooled again, and added over 10 min to a suspension of $PtCl_2(SMe_2)_2$ in dry diethyl ether (7 mL) cooled to 0 °C. The mixture was stirred for 1 h and quenched with aqueous NH_4Cl (1 mL). Extraction with diethyl ether (3 × 15 mL) and water (2 × 15 mL) produced an off-white organic phase, which was dried with $MgSO_4$ and treated with charcoal. Filtration and evaporation of the solvent produced an off-white powder (202 mg, 49%). ^{1}H NMR (200 MHz, C_6D_6): δ 1.57 (s, 12 H, S-*Me*). The extent of deuteration is estimated to be better than 95% based on the ^{1}H NMR spectrum.

[ArN═C(Me)−C(Me)═NAr]PtPh$_2$ [Ar = 2,6-Me$_2$C$_6$H$_3$] (1a). The diimine (180 mg, 0.65 mmol) was added to a solution of $Ph_2Pt(SMe_2)_2$ (290 mg, 0.61 mmol) in toluene (10 mL). The mixture was stirred for 4 h before filtration and the removal of the solvent in vacuo. The residue was dissolved in dichloromethane (20 mL), and the solution was filtered. Addition of pentane (30 mL) precipitated the product as a dark powder. Recrystallization from dichloromethane/pentane resulted in the formation of a dark purple microcrystalline solid (216 mg, 0.34 mmol, 55%). X-ray quality crystals were grown from a dichloromethane solution that was layered with pentane. ^{1}H NMR (300 MHz, CD_2Cl_2): δ 1.64 (s, 6 H, N═C*Me*), 2.22 (s, 12 H, Ar-*Me*$_o$), 6.41 (m, 2 H, Ph-*H*$_p$), 6.51 (m, 4 H, Ph-*H*$_m$), 6.88 (d, ^3J(H−H) = 6.8 Hz, ^3J(^{195}Pt−H) = 69.9 Hz, 4 H, Ph-*H*$_o$), 6.9 (m, 6 H, Ar-*H*$_{m,p}$). ^{13}C NMR (75 MHz, CD_2Cl_2): δ 17.8, 20.1 (^3J(^{195}Pt−C) = 14.0 Hz), 121.0 (^2J(^{195}Pt−C) = 13.4 Hz), 125.6 (^1J(^{195}Pt−C) = 81.1 Hz), 126.2, 128.0, 128.3, 137.1 (^2J(^{195}Pt−C) = 32.2 Hz), 144.0, 145.6, 172.6. ^{195}Pt{^{1}H} NMR (107 MHz, CD_2Cl_2): δ −3050; λ_{max} (MeCN/CH_2Cl_2, 1/10) 557 (4.29), 521 (4.42), 362 (9.15). Anal. Calcd for $C_{32}H_{34}N_2Pt$: C, 59.89; H, 5.34; N, 4.37; Pt, 30.40. Found: C, 59.57; H, 5.58; N, 4.30; Pt, 30.31.

[ArN═C(Me)−C(Me)═NAr]Pt(C$_6$D$_5$)$_2$ [Ar = 2,6-Me$_2$C$_6$H$_3$] (1a-*d*$_{10}$). The diimine (123 mg, 0.42 mmol) was added to a solution of $(C_6D_5)_2Pt(SMe_2)_2$ (202 mg, 0.42 mmol) in toluene (8 mL). The mixture was stirred for 3 h, before filtration and solvent removal in vacuo. The residue was dissolved in dichloromethane (10 mL) and filtered, and addition of pentane (15 mL) precipitated the product as a dark purple powder. Recrystallization from dichloromethane/pentane furnished the microcrystalline product (272 mg, 80%).

[ArN═C(Me)−C(Me)═NAr]PtPh$_2$ [Ar = 2,4,6-Me$_3$C$_6$H$_2$] (1b). The diimine (484 mg, 1.55 mmol) was added to a solution of $Ph_2Pt(SMe_2)_2$ (616 mg, 1.30 mmol) in toluene (20 mL). The mixture was stirred for 21 h, filtered, and the solvent was removed in vacuo. The residue was washed several times with pentane. This resulted in a dark purple microcrystalline solid (338 mg, 39%). X-ray quality crystals were grown from a dichloromethane solution that was layered with heptane. ^{1}H NMR (300 MHz, CD_2Cl_2): δ 1.63 (s, 6 H, N═C*Me*), 2.14 (s, 12 H, Ar-*Me*$_o$), 2.19 (s, 6 H, Ar-*Me*$_p$), 6.43 (m, 2 H, Ph-*H*$_p$), 6.51 (m, 4 H, Ph-*H*$_m$), 6.71 (s, 4 H, Ar-*H*$_m$), 6.84 (m, ^3J(^{195}Pt−H) = 69.7 Hz, 4 H, Ph-*H*$_o$). ^{13}C{^{1}H} NMR (75 MHz, CD_2Cl_2): δ 17.7, 20.0, 20.8, 120.9, 125.6, 128.0, 128.5, 135.8, 137.2, 143.3, 144.0, 172.7. ^{195}Pt{^{1}H} NMR (107 MHz, CD_2Cl_2): δ −3051. Anal. Calcd for $C_{34}H_{38}N_2Pt$: C, 60.97; H, 5.72; N, 4.18. Found: C, 60.98; H, 5.54; N, 4.04.

[ArN═C(Me)−C(Me)═NAr]PtPh$_2$ [Ar = 4-Br-2,6-Me$_2$C$_6$H$_2$] (1c). The diimine (159 mg, 0.35 mmol) was added to a solution of $Ph_2Pt(SMe_2)_2$ (152 mg, 0.32 mmol) in toluene (10 mL). The mixture was stirred for 18 h, and the solvent was removed in vacuo. The residue was dissolved in dichloromethane (10 mL) and filtered. The microcrystalline dark purple product was precipitated upon addition of pentane (20 mL). The solvent was decanted, and the product was dried under vacuum (137 mg, 53%). ^{1}H NMR (500 MHz, CD_2Cl_2): δ 1.62 (s, 6 H, N═C*Me*), 2.16 (s, 12 H, Ar-*Me*), 6.48 (m, 2 H, Ph-*H*$_p$), 6.56 (m, 4 H, Ph-*H*$_m$), 6.84 (m, ^3J(^{195}Pt−H) = 70.2 Hz, 4 H, Ph-*H*$_o$), 7.85 (br m, 4 H, Ar-*H*$_m$). ^{13}C{^{1}H} NMR (125 MHz, CD_2Cl_2): δ 17.6 (Ar-*Me*$_o$), 20.3 (N═C*Me*), 119.1, 121.4 (Ph-*C*$_p$), 126.0 (^3J(^{195}Pt−C) = 80.7 Hz, Ph-*C*$_m$), 130.6, 130.7, 136.8 (^2J(^{195}Pt−C) = 31.2 Hz, Ph-*C*$_o$), 143.1, 144.5, 172.9 (Ar-*C*$_p$). ^{195}Pt{^{1}H} NMR (107 MHz, CD_2Cl_2): δ −3008. Anal. Calcd for $C_{32}H_{32}Br_2N_2Pt$: C, 48.07; H, 4.03; N, 3.50. Found: C, 48.12; H, 3.89; N, 3.45.

[ArN═C(Me)−C(Me)═NAr]PtPh$_2$ [Ar = 3,5-Me$_2$C$_6$H$_3$] (1d). The diimine (484 mg, 1.55 mmol) was added to a solution of $Ph_2Pt(SMe_2)_2$ (715 mg, 1.51 mmol, not purified) in toluene (20 mL). The mixture was stirred for 21 h, and the solvent was removed in vacuo. The residue was dissolved in dichloromethane (30 mL) and filtered, and the dichloromethane was removed in vacuo. The dark purple powder was washed several times with pentane to produce the pure product (338 mg, 39% based on $PtCl_2(SMe_2)_2$ for the overall two-step synthesis). X-ray quality crystals were grown from a solution in dichloromethane that was layered with heptane. ^{1}H NMR (200 MHz, CD_2Cl_2): δ 1.89 (s, 6 H, N═C*Me*), 2.13 (s, 12 H, Ar-*Me*), 6.36 (br, 4 H, Ar-*H*$_o$), 6.45−6.59 (m, 6 H, Ph-*H*$_{m,p}$), 6.67 (br, 2 H, Ar-*H*$_p$), 6.80 (br m, 4 H, ^3J(^{195}Pt−H) = 72 Hz, Ph-*H*$_o$). ^{195}Pt{^{1}H} NMR (107 MHz, CD_2Cl_2): δ −3133. Anal. Calcd for $C_{32}H_{34}N_2Pt$: C, 59.89; H, 5.34; Pt, 30.40. Found: C, 60.22; H, 5.84; Pt, 30.00.

[ArN═C(Me)−C(Me)═NAr]PtPh$_2$ [Ar = 4-CF$_3$C$_6$H$_4$] (1e). The diimine (193 mg, 0.52 mmol) was added to a solution of $Ph_2Pt(SMe_2)_2$ (242 mg, 0.51 mmol) in toluene (10 mL). The mixture was stirred for 18 h, and the solvent was removed in vacuo. The residue was dissolved in dichloromethane (10 mL) and filtered. The microcrystalline dark purple product (62 mg, 17%) was precipitated by addition of pentane (20 mL). ^{1}H NMR (300 MHz, CD_2Cl_2): δ 1.85 (s, 6 H, N═C*Me*), 6.50 (br m, 6 H, Ph-*H*$_{m,p}$), 6.73 (m, ^3J(^{195}Pt−H) = 69.8 Hz, 4 H, Ph-*H*$_o$), 6.89 (d, 4 H, Ar-*H*), 7.40 (d, 4 H, Ar-*H*). ^{13}C{^{1}H} NMR (75 MHz, CD_2Cl_2): δ 21.5 (N═C*Me*), 121.7 (Ph-*C*$_p$), 122.7 (Ar-*C*), 125.8, 125.9 (Ar-*C*), 126.0, 126.4 (Ph-*C*$_m$), 126.9, 137.4 (Ph-*C*$_o$), 143.1, 173.3. ^{19}F-{^{1}H} NMR (188 MHz, CD_2Cl_2): δ −62.7. ^{195}Pt{^{1}H} NMR (107 MHz, CD_2Cl_2): δ −3061. Anal. Calcd for $C_{30}H_{24}F_6N_2Pt$: C, 49.93; H, 3.35; N, 3.88. Found: C, 50.30; H, 2.77; N, 4.78.

[ArN═C(Me)−C(Me)═NAr]Pt(Ph)(MeCN)$^+$OTf$^-$ [Ar = 2,6-Me$_2$C$_6$H$_3$] (2a·OTf). HOTf (30 μL, 0.34 mmol) was added dropwise to a stirred solution of **1a** (116 mg, 0.18 mmol) in MeCN at 0 °C. Stirring for 10 min produced a bright orange solution. An orange oil was obtained after removal of the solvent under vacuum. Repeated washing with diethyl ether produced an orange solid. The product was recrystallized from chloroform/pentane (102 mg, 75%). ^{1}H NMR (200 MHz, CD_2Cl_2): δ 1.88 (s, ^4J(^{195}Pt−H) = 12.9 Hz, 3 H, N═C*Me*), 2.13 (s, ^4J(^{195}Pt−H) = 10.8 Hz, 3 H, N═C*Me*′), 2.17 (s, 6 H, Ar-*Me*), 2.24 (s, 3 H, *Me*CN), 2.41 (s, 6 H, Ar-*Me*′), 6.58−6.75 (m, 5 H, *Ph*), 6.85−7.02 (m, 3 H, Ar-*H*), 7.20−7.36 (m, 3 H, Ar-*H*′). Anal. Calcd for $C_{29}H_{32}F_3N_3O_3PtS$: C, 46.15; H, 4.27; N, 5.57; Pt, 25.85. Found: C, 46.30; H, 4.32; Pt, 25.90; N, 5.82. ESI MS *m*/*z*: 605.1 (M^+).

In situ Characterization of 2a as the BF_4^- Salt. ^{1}H NMR (300 MHz, CD_2Cl_2): δ 2.05 (s, 3 H, N═C*Me*), 2.13 (s, 6 H, Ar-*Me*), 2.16 (s, 3 H, N═C*Me*′), 2.37 (s, 6 H, Ar-*Me*′), 6.57−6.71 (m, 5 H, *Ph*), 6.83−6.89 (m, 3 H, Ar-*H*), 7.19−7.32 (m, 3H, Ar-*H*′).

In situ Characterization of 2a Obtained from Protonation of 1a with HOTf at −78 °C, Decomposition at 0 °C, and Addition of

(127) Song, D.; Wang, S. *J. Organomet. Chem.* **2002**, *648*, 302−305.

CD_3CN (0.1 mL). ^{1}H NMR (200 MHz, CD_2Cl_2): δ 2.02 (s, 3 H, N=C*Me*), 2.12 (s, 6 H, Ar-*Me*), 2.13 (s, 3 H, N=C*Me*′), 2.36 (s, 6 H, Ar-*Me*′), 6.57−6.71 (m, 5 H, *Ph*), 6.83−6.89 (m, 3 H, Ar-*H*), 7.19−7.32 (m, 3 H, Ar-*H*′).

NMR-Tube Generation of [ArN=C(Me)−C(Me)=NAr]Pt(C_6D_5)(CD_3CN)$^+BF_4^-$ [Ar = 2,6-$Me_2C_6H_3$] (2a-d_5·BF_4). After the EXSY measurements on the protonated **1a-d_{10}** (see below), the sample was heated to room temperature, and CD_3CN (100 μL) was added. ^{1}H NMR (500 MHz, CD_2Cl_2): δ 2.03 (s, 3 H, N=C*Me*), 2.14 (s, 9 H, Ar-*Me* and N=C*Me*′), 2.37 (s, 6 H, Ar-*Me*′), 6.85−7.02 (m, 3 H, Ar-*H*), 7.20−7.36 (m, 3 H, Ar-*H*′).

[ArN=C(Me)−C(Me)=NAr]Pt(Ph)(MeCN)$^+$OTf$^-$ [Ar = 2,4,6-$Me_3C_6H_2$] (2b·OTf). The compound was prepared analogous to **2a** above from HOTf (10 μL, 012 mmol) and **1b** (50 mg, 0.075 mmol). The product was recrystallized from dichloromethane/pentane (55 mg, 94%). ^{1}H NMR (300 MHz, CD_2Cl_2): δ 1.89 (s, $^4J(^{195}Pt-H)$ = 11.3 Hz, 3 H, N=C*Me*), 2.10 (s, 6 H, *o*-Ar-*Me*), 2.11 (s, 3 H, N=C*Me*′), 2.17 (s, 3 H, *p*-Ar-*Me*′), 2.20 (s, 3 H, *Me*CN), 2.35 (s, 6 H, *o*-Ar-*Me*′), 2.38 (s, 3 H, *p*-Ar-Me), 6.60−6.69 (m, 5 H, *Ph*), 6.71 (m, 2 H, Ar-*H*), 7.11 (m, 2 H, Ar-*H*′). Anal. Calcd for $C_{31}H_{36}F_3N_3O_3PtS$: C, 47.57; H, 4.64; N, 5.37; Pt, 24.92. Found: C, 46.70; H, 4.71; N, 5.10; Pt, 24.09. ESI MS *m*/*z*: 633.3 (M^+).

NMR-Tube Generation of [ArN=C(Me)−C(Me)=NAr]Pt(Ph)(CD_3CN)$^+BF_4^-$ [Ar = 4-Br-2,6-$Me_2C_6H_2$] (2c·BF_4). HBF_4·Et_2O (10 μL) was added to an NMR tube containing **1c** (3 mg) in CD_2Cl_2 (400 μL) with added CD_3CN (100 μL). Shaking turned the deep purple solution bright orange. ^{1}H NMR (200 MHz, CD_2Cl_2): δ 2.05 (s, 3 H, $^4J(^{195}Pt-H)$ = 10.8 Hz, N=C*Me*), 2.11 (s, 6 H, Ar-*Me*), 2.14 (s 3 H, N=C*Me*′), 2.35 (s, 6 H, Ar-*Me*′), 6.67 (s, 5 H, Ph-$H_{m,o,p}$), 7.03 (s, 2 H, Ar-*H*), 7.33 (s, 6 H, C_6H_6), 7.45 (s, 2 H, Ar-*H*′). ES MS *m*/*z*: 764.2 (M^+).

NMR-Tube Generation of [ArN=C(Me)−C(Me)=NAr]Pt(Ph)(CD_3CN)$^+BF_4^-$ [Ar = 3,5-$Me_2C_6H_3$] (2d·BF_4). HBF_4·Et_2O (5 μL) was added to an NMR tube containing **1d** (3 mg) in CD_2Cl_2 (400 μL) with added CD_3CN (100 μL). Shaking turned the deep purple solution bright orange. ^{1}H NMR (200 MHz, CD_2Cl_2): δ 2.07 (s, 6 H, Ar-*Me*), 2.11 (s, 3 H, N=C*Me*), 2.19 (s, 3 H, N=C*Me*), 2.39 (s, 6 H, Ar-*Me*′), 6.27 (s, 2 H, Ar-H_o), 6.5−6.7 (m, 5 H, Ph-*H*), 6.77 (s, 2 H, Ar-H_o′), 7.05 (s, 1 H, Ar-H_p), 7.32 (s, 7 H, C_6H_6 + Ar-H_p′). ESI MS *m*/*z*: 605.4 (M^+).

In situ Characterization of Product after Protonation of 1d at Low Temperature, Decomposition at 0 °C, and Addition of CD_3CN (0.1 mL). ^{1}H NMR (200 MHz, CD_2Cl_2): δ 2.07 (s, 6 H, Ar-*Me*), 2.12 (s, 6 H, N=C*Me*), 2.20 (s, 3 H, N=C*Me*′), 2.39 (s, 6 H, Ar-*Me*′), 6.28 (s, 2 H, Ar-H_o), 6.5−6.7 (m, 5 H, Ph-*H*), 6.79 (s, 2 H, Ar-H_o′), 7.04 (s, 1 H, Ar-H_p), 7.31 (s, 7 H, C_6H_6 + Ar-H_p′).

NMR-Tube Generation of [ArN=C(Me)−C(Me)=NAr]Pt(Ph)(CD_3CN)$^+BF_4^-$ [Ar = 4-$CF_3C_6H_4$] (2e·BF_4). HBF_4·Et_2O (5 μL) was added to an NMR tube containing **1e** (3 mg) in CD_2Cl_2 (400 μL) with added CD_3CN (100 μL). Shaking turned the deep purple solution bright orange. ^{1}H NMR (200 MHz, CD_2Cl_2): δ 2.14 (s, 3 H, $^4J(^{195}Pt-H)$ = 10.4 Hz, N=C*Me*), 2.23 (s 3 H, N=C*Me*′), 6.5−6.8 (m, 5 H, Ph-$H_{m,o,p}$), 6.92 (d, 2 H, Ar-*H*), 7.40 (d, 2 H, Ar-*H*), 7.43 (d, 2 H, Ar-*H*), 7.89 (d, 2 H, Ar-*H*). ESI MS *m*/*z*: 685.2 (M^+).

Low-Temperature Protonation of 1a in the Presence of Acetonitrile. Characterization of [ArN=C(Me)−C(Me)=NAr]Pt(H)(Ph)$_2$($MeCN$)$^+$OTf$^-$ [Ar = 2,6-$Me_2C_6H_3$] (3a·OTf). The cationic Pt(IV) hydride was prepared by the protonation procedure described below, and the characterization was done in situ. ^{1}H NMR (300 MHz, CD_2Cl_2): δ −21.47 (s, $^1J(^{195}Pt-H)$ = 1597 Hz, 1 H, Pt-*H*), 2.03 (s, 6 H), 2.16 (s, 6 H), 2.41 (s, 6 H), 3.59 (s, 3 H, *Me*CN), 6.54 (m, 4 H, Ph-*H*), 6.72 (m, 6 H, Ph-*H*), 6.94 (m, 6 H, Ar-*H*).

Low-Temperature Protonation of (N−N)$PtPh_2$ (1) in the Absence of Acetonitrile: General Procedure. This procedure is a modification of procedures previously described by us.[60] A solution of **1a−c** (ca. 10 mg, ca. 20 μmol) in CD_2Cl_2 (400 μL) in an NMR tube was carefully layered with CD_2Cl_2 (100 μL). (The layering technique was used to prevent premature mixing of **1** and acid.) The contents were cooled to −78 °C and carefully layered with a solution of HBF_4·Et_2O (13 μL, ca. 5 equiv) in a mixture of Et_2O-d_{10} (73 μL, 1 M) and CD_2Cl_2 (120 μL), giving a total volume of ca. 700 μL. The tube was capped and kept at −78 °C. The tube was shaken in order to mix the reactants immediately before it was transferred to a precooled NMR probe. A pale yellow solution was immediately obtained. Particular care was taken to minimize any heating of the sample, which appeared homogeneous at all times. The product distributions observed at −40 °C are not very different from those at −78 °C, suggesting that unintentional heating did not perturb the outcome of the experiments.

Characterization of [ArN=C(Me)−C(Me)=NAr]Pt(C_6H_6)(Ph)$^+$ Cations as Their BF_4^- Salts (4·BF_4). The π-benzene cations were prepared by the protonation procedure described above, and characterization was done in situ by ^{1}H NMR, NOESY, EXSY, COSY and HMQC.

[ArN=C(Me)−C(Me)=NAr]Pt(C_6H_6)(Ph)$^+$ [Ar = 2,6-$Me_2C_6H_3$] (4a). ^{1}H NMR (500 MHz, T = −43 °C, CD_2Cl_2): δ 1.99 (s, 3 H, NC*Me*), 2.12 (s, 6 H, Ar-*Me*), 2.14 (s, 3 H, NC*Me*), 2.44 (s, 6 H, Ar-*Me*), 6.11−6.28 (m, 2 H, Ph-H_o), 6.71 (m, 3 H, Ar-$H_{m,p}$), 6.85 (s, 6 H, C_6H_6), 7.25 (m, 3 H, Ar-$H_{m,p}$); λ_{max} (CH_2Cl_2/MeCN(10% v/v)) 391 (4.27), 320 (8.14).The spectrum of **4a−d_{10}** was identical except that the benzene and phenyl ligands were only ca. 10% of the intensity seen in **4a**.

[ArN=C(Me)−C(Me)=NAr]Pt(C_6H_6)(Ph)$^+$ [Ar = 2,4,6-$Me_2C_6H_2$] (4b). ^{1}H NMR (500 MHz, T = −18 °C, CD_2Cl_2): δ 1.99 (ds, 6 H, NC*Me* + Ar-Me_p), 2.06 (s, 6 H, Ar-Me_o), 2.14 (s, 3 H, NC*Me*′), 2.31 (s, 3 H, Ar-Me_p′), 2.40 (s, 6 H, Ar-Me_o′), 6.16 (m, 4 H, Ph-$H_{o,m}$), 6.27 (m, 1 H, Ph-H_p), 6.46 (s, 2 H, Ar-H_m), 6.88 (sb, 6 H, C_6H_6), 7.09 (s, 2 H, Ar-H'_m).

[ArN=C(Me)−C(Me)=NAr]Pt(C_6H_6)(Ph)$^+$[Ar=4-Br-2,6-$Me_2C_6H_2$] (4c). ^{1}H NMR (500 MHz, T = −48 °C, CD_2Cl_2): δ 2.01 (s 3 H, NC*Me*), 2.08 (s, 6 H, Ar-*Me*), 2.16 (s, 3 H, NC*Me*′), 2.42 (s, 6 H, Ar-*Me*′), 6.17 (sb, 4 H, Ph-$H_{o,m}$), 6.31 (sb, 1 H, Ph-H_p), 6.78 (s, 2 H, Ar-H_m), 6.86 (s, 6 H, C_6H_6), 7.42 (s, 2 H, Ar-H_m′).

[ArN=C(Me)−C(Me)=NAr]Pt(C_6H_6)(Ph)$^+$ [Ar = 3,5-$Me_2C_6H_3$] (4d). ^{1}H NMR (500 MHz, T = −73 °C, CD_2Cl_2): δ 1.93 (s, 3 H, Ar-*Me*), 2.04 (s, 3 H, NC*Me*), 2.13 (s, 3 H, NC*Me*), 2.35 (s, 6 H, Ar-*Me*), 6.07 (mb, 5 H, Ph-$H_{o,m}$ + Ar-H_p), 6.18 (mb, 1 H, Ph-H_p), 6.44 (d, 1 H, Ar-H_p), 6.83 (mb, 2 H, Ar-H_m), 6.97 (s, 8 H, C_6H_6 + Ar-H_m).

[ArN=C(Me)−C(Me)=NAr]Pt(C_6H_6)(Ph)$^+$ [Ar = 4-$CF_3C_6H_4$] (4e). ^{1}H NMR (500 MHz, T = −53 °C, CD_2Cl_2): δ 2.07 (s, 3 H, NC*Me*), 2.18 (s, 3 H, NC*Me*), 6.02−6.11 (mb, 4 H, Ph-$H_{o,m}$), 6.21 (mb, 1 H, Ph-H_p), 6.79 (d, 2 H, Ar-*H*), 6.96 (s, 6 H, C_6H_6), 7.14 (d, 2 H, Ar-*H*), 7.57 (d, 2 H, Ar-*H*), 7.87 (d, 2 H, Ar-*H*).

SST Measurements. The SST experiments were acquired with a modification of the zghd pulse program supplied with the Bruker Avance DPX/DRX Spectrometers. The T_1 relaxation was measured by the inversion recovery method for each temperature and used in the calculation of the rate constants. The power level of the saturation pulse was adjusted before each temperature.

EXSY Spectroscopy. After protonation and transfer of the sample to the precooled NMR probe, the 2D EXSY spectra were recorded using a gradient-selected NOESY pulse program from Bruker (noesygpph). All spectra were recorded at 500.13 MHz with mixing time, τ_m, optimized for each temperature.[54] The spectra were recorded with a sweep width of 8.2 ppm, 4096 data points in the *F*2 direction, 256 increments in the *F*1 direction, and 2 transients per increment, and a relaxation delay of 3 s. This setup produced a total acquisition time of approximately 40 min depending on τ_m. The spectra were apodized with a qsine function and zero-filled to give a 2048 × 2048 matrix. The spectra were phased to give positive peaks along the diagonal.

The basis for the extraction of kinetic and thermodynamic data produced by the EXSY experiments is integration of the cross-peak volumes of the EXSY NMR spectra. The integration of the 2D spectra was performed using two different software applications, Xwinnmr[128]

and MestReC,[129] as an extra consistency and quality control of the data. From the integrals (I) of the cross-peaks and the diagonal peaks and the mole fractions (X) of the two exchanging spins (0.5:0.5 when using the ligand symmetrization as the basis), it is possible to calculate the r values as defined below. These are then used together with the mixing time (τ_m) of the 2D EXSY experiment to calculate the rate constant, k, of the exchange process.[54]

$$r = \frac{4X_aX_b(I_{AA} + I_{BB})}{I_{AB} + I_{BA}} - (X_a - X_b)^2$$

$$k = \frac{1}{\tau_m}\ln\frac{(r+1)}{(r-1)}$$

X-ray Crystallographic Structure Determination of 1a, 1b, 1d, 2a, and 2b. Crystals of **1a** were grown from dichloromethane/pentane, whereas **1b**, **1d**, **2a**, and **2b** were grown from dichloromethane/heptane. The crystals were mounted on glass fiber with perfluoropolyether, and the data were collected at 105 K on a Siemens 1K SMART CCD diffractometer using graphite-monochromated Mo Kα radiation. Data collection method: ω-scan, range 0.3°, crystal to detector distance 5 cm. Data reduction and cell determination were carried out with the SAINT and XPREP[130] programs. Absorption corrections were applied by the use of the SADABS[131] program. All the structures were solved using the Sir92[132] or Sir97[133] programs and refined on F using the program Crystals.[134]

The non-hydrogen atoms were refined with anisotropic thermal parameters; the H atoms were all located in a difference map, but those attached to carbon atoms were repositioned geometrically. The H atoms were initially refined with soft restraints on the bond lengths and angles to regularize their geometry (C−H in the range 0.93−98 Å) and isotropic adps (U(H) in the range 1.2−1.5 × U_{equiv} of the adjacent atom), after which they were refined with riding constraints. Table 1 lists the experimental and crystallographic data. Selected bond lengths, angles, and torsion angles are given in Table 2. Crystallographic data for all five compounds may be obtained as individual CIF files in the Supporting Information.

Acknowledgment. We gratefully acknowledge the Norwegian research council for generous stipends to B.J.W., M.L., and A.K. We thank Cynthia M. Norris for generously providing the SST pulse program.

Supporting Information Available: Crystallographic data for **1a**, **1b**, **1d**, **2a**, and **2b** in CIF format. This material is available free of charge via the Internet at http://pubs.acs.org.

JA056694Z

(128) *XWinNMR:* Bruker Spectrospin Gmbd.
(129) Available at http://www.mestrec.com/.
(130) *SMART and SAINT*, Area-detector Control and Integration Software; Siemens Industrial Automation Inc.: Madison, WI, 1995.
(131) *SADABS*, Area-Detector Absorption Correction; Siemens Industrial Automation Inc.: Madison, WI, 1996.
(132) Altomare, A.; Cascarano, G.; Giacovazzo, C.; Guagliardi, A.; Burla, M. C.; Polidori, G.; Camalli, M. *J. Appl. Crystallogr.* **1994**, *27*, 435.
(133) Altomare, A.; Burla, M. C.; Camalli, M.; Cascarano, G. L.; Giacovazzo, C.; Guagliardi, A.; Moliterni, A. G. G.; Polidori, G.; Spagna, R. *J. Appl. Crystallogr.* **1999**, *32*, 115−119.
(134) Betteridge, P. W.; Carruthers, J. R.; Cooper, R. I.; Prout, K.; Watkin, D. J. *J. Appl. Crystallogr.* **2003**, *36*, 1487.